Linear stability analysis of turbulent channel flow including porous walls

J. Jiménez G. Kawahara A. Pinelli M. Uhlmann

August 1998

Technical Note ETSIA MF-9811
Dep. Motopropulsión y Termofluidodinámica
E.T.S. Ingenieros Aeronáuticos, Universidad Politécnica de Madrid

Contents

I Turbulent channel flow over a porous wall **3**

1 Introduction **3**

2 Linear stability analysis **4**

2.1 Piecewise linear base flow 4

2.2 Turbulent-channel base flow 6

3 Numerical procedure **7**

3.1 Consistency and convergence check of the present method for plane Poiseuille flow 8

4 Results **8**

4.1 Recap of the inviscid analysis for a piecewise linear base profile 8

4.2 Viscous analysis of a turbulent base profile 9

5 Conclusions **9**

II Model flow for streak instability **13**

6 Introduction **13**

7 Linear stability analysis **13**

8 Numerical procedure **15**

Bibliography **16**

Figures **17**

A On the Reynolds–Tiederman velocity profile in a turbulent channel **24**

B B-spline expansion **26**

B.1 The present spline base 26

B.2 Analytical grid mapping 26

B.3 Galerkin procedure 27

B.4 Treatment of boundary conditions 28

B.5 Gauss elimination of boundary values 29

C Details of the streak instability problem **30**

C.1 Linear stability equations 30

C.2 Linearized mode-wise stability equations 31

C.3 The discretization of the streak instability problem 36

C.4 Numerical treatment of boundary conditions 36

D MAPLE sources for the stability problem **40**

D.1 Derivation of the streak instability equations, modewise 40

Part I

Turbulent channel flow over a porous wall

1 Introduction

The following stability analysis has been motivated by the observation of spanwise organized structures in direct numerical simulations of plane channel flow over a partially permeable wall performed by the authors. Those preliminary results, which have yet to be confirmed statistically as well as over a range of parameters, could indicate the formation of "roller" like structures perpendicular to the mean flow caused by some kind of instability mechanism of the turbulent base flow. The basic set-up of the porous wall flow can be seen in figure 1. The impermeability constraint of the lower wall of the plane channel is relaxed such that the wall normal velocity v_w in the plane $y = 0$ is generally non-zero. At the same time, the no-slip condition $u = w = 0$ is still respected by the flow in that plane. In our case, the actual value of the transpiration velocity v_w is linked to the local pressure fluctuations by Darcy's law of flow through porous media [1, p.225]. This condition can be interpreted (and technically realized) as indicated in the figure: the principal channel flow is separated from an adjacent chamber by a porous plate which allows transverse exchange of fluid. If the pressure in the chamber is adjusted to be equal to the mean flow pressure $p(x)$ of the channel, the net mass flux across the plate is zero (locally the ensemble average is also zero). The importance of this configuration lies in the fact that it could serve as a simple means of increasing drag in some technical applications, e.g. aeronautics.

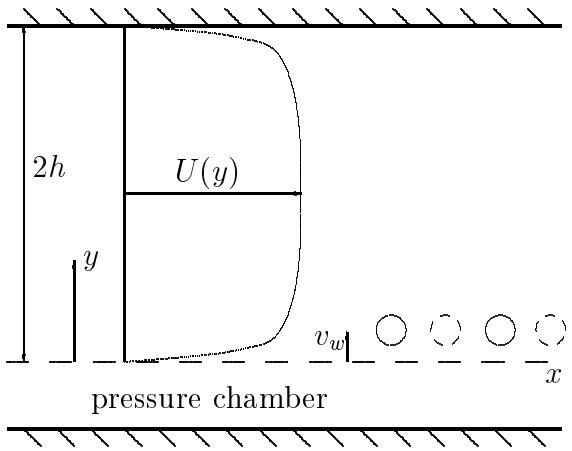

Figure 1: Schematic of plane channel flow with one porous wall and adjacent chamber that can be used to control the mean pressure drop.

In order to gain some insight into the fundamental influence of the permeability on turbulent flow, we investigate its stability characteristics in the present report. This analysis forms part of an ongoing project involving – besides the aforementioned DNS – as well the study of the rebound of a vortex dipole on partially permeable walls. It should be mentioned at this point that spanwise organisation has been one of the key features observed in simulations of somewhat similar turbulence control strategies recently published by Koumoutsakos [2], although the connection to the present work is unclear at the time being. Other authors who have recently investigated permeable walls by means of DNS are Wagner and Friedrich [3], however for the case of perfect permeability.

The outline of this report is as follows. We will first present the basic approach of our stability

analysis, applying it initially to a piecewise linear base flow inviscidly (a problem that can be tackled analytically) and then to a realistic turbulent velocity profile which requires a numerical solution. In section 3 we give the details of our numerical approach and present the results in section 4 before drawing some conclusions in section 5.

2 Linear stability analysis

In the following, we shall investigate the instability of wall-bounded two-dimensional uni-directional flows to a small disturbance. Base flows to be considered here have the velocity $\boldsymbol{U} = U(y)\boldsymbol{i}$, where $\boldsymbol{i}$, $\boldsymbol{j}$ and $\boldsymbol{k}$ represent respectively the streamwise, the wall-normal and the spanwise unit vectors, and x, y and z are used to denote the corresponding coordinates.

The motion of a two-dimensional flow $\boldsymbol{v} = u\boldsymbol{i} + v\boldsymbol{j}$ is described by the vorticity equation as

$$\partial_t \omega + (u\partial_x + v\partial_y)\omega = \nu \nabla_2^2 \omega, \tag{1}$$

where $\nabla_2^2 = \partial_x^2 + \partial_y^2$ is the two-dimesional Laplacian, ν is the kinematic viscosity, and $\omega = \partial_x v - \partial_y u$ is the spanwise vorticity which is related to the streamfunction ψ via $\nabla_2^2 \psi = -\omega$, and ψ satisfies the relations as

$$u = \partial_y \psi, \quad v = -\partial_x \psi. \tag{2}$$

Let us decompose the flow field into the contribution from the base flow and a small disturbance as

$$u(x,y,t) = U(y) + u'(x,y,t), \quad v(x,y,t) = v'(x,y,t) \quad (\psi(x,y,t) = \Psi(y) + \psi'(x,y,t)), \tag{3}$$

where $U = \partial_y \Psi$. When we substitute (3) into (1) and drop the non-linear terms with respect to the small disturbance, we have, for the disturbance part,

$$(\partial_t + U\partial_x)\nabla_2^2 \psi' - \frac{\mathrm{d}^2 U}{\mathrm{d}y^2}\partial_x \psi' - \nu \nabla_2^2 \nabla_2^2 \psi' = 0, \tag{4}$$

and this equation is supplemented by wall boundary conditions,

$$\psi = \partial_y \psi = 0 \tag{5}$$

for a normal wall, and

$$\left(\beta \frac{\mathrm{d}U}{\mathrm{d}y} - \partial_x\right)\psi' + \beta\nu\partial_y^3 \psi' = 0, \quad \psi = 0 \tag{6}$$

for a porous wall, where β denotes the porosity and we have employed the streamwise momentum equation and Darcy's law

$$v' + \beta p' = 0. \tag{7}$$

Here, p' is the disturbance pressure (mass density of the fluid has been taken as unity).

Since we can easily transform three-dimensional stability problem to two-dimensional one by using Squire's transformation, we investigate the instability of the base flow to two-dimensional disturbances throughout Part I of the present report.

2.1 Piecewise linear base flow

First, we shall consider the base flow of a piecewise linear velocity profile as

$$U(y) = \begin{cases} Sy & (0 < y < \delta) \\ S\delta & (y > \delta) \end{cases}, \tag{8}$$

which has uniform spanwise vorticity, $-S$, at $0 < y < \delta$ and has null vorticity at $y > \delta$. Figure 2 shows this piecewise linear velocity profile as well as the wave-like perturbation to be imposed. This base flow is considered to be the simplest model for a turbulent wall layer. If we neglect the viscous term, for the base flow (8), equation (4) becomes

$$(\partial_t + Sy\partial_x)\,\nabla_2^2\psi = 0 \quad (0 < y < \delta), \quad (\partial_t + S\delta\partial_x)\,\nabla_2^2\psi = 0 \quad (y > \delta). \tag{9}$$

Hereafter we drop the prime added to the disturbance in Part I.

In the following, we consider the disturbance streamfunction in the form

$$\psi(x, y, t) = \Re\left[\psi(y)\mathrm{e}^{\mathrm{i}\alpha(x-ct)}\right], \tag{10}$$

where c stands for the complex phase velocity and α is the streamwise wavenumber of the disturbance (see figure 2).

The disturbance takes a traveling-wave form similar to Tollmien–Schlichting wave. If $\Im[c] > 0$, the flow is unstable and the growth rate is given by $\alpha\,\Im[c]$. By substituting (10) to (9), we have

$$(Sy - c)\left(\frac{\mathrm{d}^2}{\mathrm{d}y^2} - \alpha^2\right)\psi = 0 \quad (0 < y < \delta), \quad (S\delta - c)\left(\frac{\mathrm{d}^2}{\mathrm{d}y^2} - \alpha^2\right)\psi = 0 \quad (y > \delta), \tag{11}$$

which have solutions as

$$\psi(y) = A_0\mathrm{e}^{-\alpha y} + B_0\mathrm{e}^{\alpha y} \quad (0 < y < \delta), \quad \psi(y) = A\mathrm{e}^{-\alpha y} \quad (y > \delta). \tag{12}$$

The latter solution decays as $y \to \infty$. Here, we have assumed that $\alpha > 0$. If c and ψ are the eigenvalue and the eigenfunction for given α (> 0), c^* and ψ^* are also the eigenvalue and the eigenfunction for $-\alpha$, where the asterisk denotes complex conjugate.

The matching conditions for the wall-normal velocity and the pressure (or equivalently the streamwise velocity) at $y = \delta$ yield

$$A_0 + \mathrm{e}^{2\alpha\delta}B_0 - A = 0, \tag{13}$$

$$(S\delta - c + S/\alpha)A_0 - (S\delta - c - S/\alpha)\mathrm{e}^{2\alpha\delta}B_0 - (S\delta - c)A = 0. \tag{14}$$

On the other hand, the inviscid (free-slip) version of the wall boundary condition (6)

$$(S\beta - \mathrm{i}\alpha)\psi + c\beta\frac{\mathrm{d}\psi}{\mathrm{d}y} = 0 \tag{15}$$

at $y = 0$ yields

$$[\alpha + \mathrm{i}\beta(S - \alpha c)]A_0 + [\alpha + \mathrm{i}\beta(S + \alpha c)]B_0 = 0. \tag{16}$$

In order that the matching and the wall boundary conditions (13), (14) and (16) have non-trivial solutions, the dimensionless eigenvalue is required as

$$\begin{aligned}\frac{\alpha c}{S} &= \tfrac{1}{2}[\alpha' + \tfrac{1}{2}(1 - \mathrm{e}^{-2\alpha'})] - \mathrm{i}\tfrac{1}{2}\frac{\alpha'}{\beta'} \\ &\pm\tfrac{1}{2}\mathrm{i}\left\{\frac{\alpha'^2}{\beta'^2} - \left[\alpha + \tfrac{1}{2}(1 - \mathrm{e}^{-2\alpha'})\right]^2 + 4\alpha' - 2(1 - \mathrm{e}^{-2\alpha'})\right. \\ &\left.+\mathrm{i}\frac{\alpha'}{\beta'}\left[-2\alpha' + 3(1 - \mathrm{e}^{-2\alpha'})\right]\right\}^{\frac{1}{2}},\end{aligned} \tag{17}$$

where

$$\alpha' = \alpha\delta, \quad \beta' = S\delta\beta \tag{18}$$

are dimensionless wavenumber and porosity, respectively.

In the case of $0 \leq \beta' \ll \alpha'$ $(0 \leq \beta'/\alpha' \ll 1)$, the asymptotic expression of (17) is given by

$$\frac{\alpha c}{S} = \alpha' - \tfrac{1}{2}(1 - \mathrm{e}^{-2\alpha'}) + \mathrm{i}\frac{\beta'}{\alpha'}\mathrm{e}^{-2\alpha'}\left[\alpha' - \tfrac{1}{2}(1 - \mathrm{e}^{-2\alpha'})\right], \tag{19}$$

the imaginary part of which behaves as

$$\frac{\alpha \Im[c]}{S} \approx \begin{cases} \beta'\alpha' & (\alpha' \ll 1) \\ \beta'\mathrm{e}^{-2\alpha'} & (\alpha' \gg 1) \end{cases}. \tag{20}$$

The dimensionless maximum growth rate is around $0.140\beta'$, and the most unstable dimensionless wave number is around 0.386. In the case of $0 \leq \alpha' \ll \beta'$ $(0 \leq \alpha'/\beta' \ll 1)$, the asymptotic expression of (17) is given by

$$\frac{\alpha c}{S} = \tfrac{1}{2}\left[\alpha' + \tfrac{1}{2}(1 - \mathrm{e}^{-2\alpha'})\right] - \tfrac{1}{4}\frac{\alpha'}{\beta'}\left[-2\alpha' + 3(1 - \mathrm{e}^{-2\alpha'})\right] R^{-\frac{1}{2}} + \tfrac{1}{2}\mathrm{i}R^{\frac{1}{2}} - \tfrac{1}{2}\mathrm{i}\frac{\alpha'}{\beta'}, \tag{21}$$

where

$$R = -\left[\alpha'^2 + \tfrac{1}{2}(1 - \mathrm{e}^{-2\alpha'})\right]^2 + 4\alpha' - 2(1 - \mathrm{e}^{-2\alpha'}). \tag{22}$$

The imaginary part of the leading term behaves as

$$\frac{\alpha \Im[c]}{S} \approx \begin{cases} \dfrac{1}{\sqrt{3}}\alpha'^{\frac{3}{2}} & (\alpha' \ll 1) \\ 0 & (\alpha' > 1.83) \end{cases}. \tag{23}$$

The dimensionless maximum growth rate is around 0.246, and the most unstable dimensionless wave number is around 1.23.

In the special cases, i.e., an impermeable wall ($\beta' = 0$) and a perfectly permeable wall ($\beta' = \infty$), we have, from (19) and (21),

$$\frac{\alpha c}{S} = \alpha' - \tfrac{1}{2}(1 - \mathrm{e}^{-2\alpha'}) \tag{24}$$

and

$$\frac{\alpha c}{S} = \tfrac{1}{2}\left[\alpha' + \tfrac{1}{2}(1 - \mathrm{e}^{-2\alpha'})\right] + \tfrac{1}{2}\mathrm{i}R^{\frac{1}{2}}, \tag{25}$$

respectively. Equation (24) tells us that the flow over an impermeable wall is neutrally stable. Eigenvalue (25) coincides with that for a wake (see figure 3) with a piecewise linear velocity profile as

$$U(y) = \begin{cases} S\delta & (y < -\delta) \\ -Sy & (-\delta < y < 0) \\ Sy & (0 < y < \delta) \\ S\delta & (y > \delta) \end{cases}. \tag{26}$$

2.2 Turbulent-channel base flow

Next, we shall consider the base flow of the turbulent-channel velocity profile proposed by Reynolds & Tiederman [4] as

$$\frac{\mathrm{d}U}{\mathrm{d}y} = -\frac{Re_\tau y}{1 + G(y)} \quad (0 < y < 2), \tag{27}$$

$$G(y-1) = \tfrac{1}{2}\left\{1 + \left[\frac{KRe_\tau}{3}(1 - y^2)(1 + 2y^2)\left(1 - \exp\left(-\frac{(1+y)Re_\tau}{A}\right)\right)\right]^2\right\}^{\frac{1}{2}} - \tfrac{1}{2}, \tag{28}$$

where $K = 0.525$, $A = 37$, and

$$Re_\tau = \frac{u_\tau h}{\nu} \tag{29}$$

is a Reynolds number based on friction velocity u_τ and channel half-width h. Here, y is normalized by h, and the value of Reynolds number is taken as $Re_\tau = 180$. The profile is symmetrized about $y = 1$. Note that for this base flow there are no unstable eigenmodes of the linearized Navier–Stokes equations with normal wall conditions (5).

When we consider the disturbance streamfunction (10), equation (4) is rewritten in the dimensionless form as

$$\left[(U-c)\left(\frac{\mathrm{d}^2}{\mathrm{d}y^2}-\alpha^2\right)-\frac{1}{\mathrm{i}\alpha Re_\tau}\left(\frac{\mathrm{d}^2}{\mathrm{d}y^2}-\alpha^2\right)^2-\frac{\mathrm{d}^2U}{\mathrm{d}y^2}\right]\psi=0, \tag{30}$$

where we have used u_τ and h as representative velocity and length. The porous-wall conditions (see (6))

$$\left(\beta\frac{\mathrm{d}U}{\mathrm{d}y}-\mathrm{i}\alpha\right)\psi+\frac{\beta}{\mathrm{i}\alpha Re_\tau}\frac{\mathrm{d}^3\psi}{\mathrm{d}y^3}=0, \quad \frac{\mathrm{d}\psi}{\mathrm{d}y}=0 \tag{31}$$

are imposed at $y = 0$, while the normal-wall conditions (see (5))

$$\psi=\frac{\mathrm{d}\psi}{\mathrm{d}y}=0 \tag{32}$$

are imposed at $y = 2$.

3 Numerical procedure

Using the method of weighted residuals (MWR), the stability problem (30) can be formulated as follows:

$$\int_\Omega\left[(U(y)-c)\left(\frac{\mathrm{d}^2}{\mathrm{d}y^2}-\alpha\right)-\frac{1}{i\alpha\mathrm{Re}}\left(\frac{\mathrm{d}^2}{\mathrm{d}y^2}-\alpha\right)^2-\frac{\mathrm{d}^2U(y)}{\mathrm{d}y^2}\right]\psi(y)\cdot\Psi_k\,\mathrm{d}\Omega\;=\;0\,, \tag{33}$$

where Ω is the computational domain and Ψ_k are the test functions. Similarly, the approximate solution is represented by a projection upon a series of trial functions Φ_l, viz.

$$\psi(y)\;=\;\sum_{l=1}^{N}\hat{\psi}_l\cdot\Phi_l(y)\quad, \tag{34}$$

where $\hat{\psi}_l$ are the coefficients of the expansion. We resort to a Galerkin method, thus $\Psi_l = \Phi_l$, furthermore choosing b-splines as the expanion functions. The order of the b-spline polynomial functions is fixed at 6 throughout this work. Details of the particular base chosen can be found in appendix B.

Inserting the expansion (34) into our sytem of equations (33) and evaluating the involved integrals (see appendix B.3 for details) leads to the following system of discretized equations:

$$\begin{aligned}\left\{-\frac{1}{i\alpha\mathrm{Re}}M_{40}\;-\;\widetilde{M}(\hat{U})\;+\;\widetilde{K}(\hat{U})\;-\;\alpha^2\,\widetilde{\widetilde{M}}(\hat{U})\;+\;\frac{2\alpha}{i\mathrm{Re}}K\;-\;\frac{\alpha^3}{i\mathrm{Re}}M\right\}\hat{\psi}\;=\\ c\,\left\{K\;-\;\alpha^2\,M\right\}\,\hat{\psi}\end{aligned} \tag{35}$$

The matrices M_{40}, $\widetilde{M}(\hat{U})$, $\widetilde{K}(\hat{U})$, $\widetilde{\widetilde{M}}(\hat{U})$, $\widetilde{\widetilde{M}}(\hat{U})$, K and M appearing in the above system (35) are of $(2k-1)$-banded structure and can be precalculated depending only on the base profile $U(y)$ and the spline base of order N chosen.

The above system has thus the structure

$$A\cdot\hat{\psi}\;=\;c\cdot B\cdot\hat{\psi}\quad, \tag{36}$$

with the obvious definition of the system matrices A and B. The boundary conditions of our specific flow problem (see section 2.2) will be written directly into matrices A, B once they are assembled according to the above definitions. This procedure constitutes thus a Galerkin-tau method [5]. The exact implementation of the discretized boundary conditions is given in appendix B.4.

Performing the eigensystem analysis of equation (36) requires solving the complex generalized eigenvalue problem $|A - \lambda B| = 0$ for the eigenvalues λ which can be done by using standard library routines (e.g. LAPACK or EISPACK [6]). In order to prevent the appearance of spurious eigenvalues that might be caused by the boundary treatment through the tau method, on can use a partial Gauss elimination procedure suggested by Mizushima [7] prior to the eigensystem analysis. Further details are given in appendix B.5. Subsequently computing associated right eigenvectors $\vec{r}^i$ simply requires solving the linear system $(A - \lambda_i B)\vec{r}^i = 0$. Since this system of equations is overdetermined, one element of $\vec{r}^i$ has to be chosen freely (unity, say). It should be noted that, contrary to the eigenvalues which are invariant to a change of base, the obtained eigenvectors need to be retransformed to physical space by the inverse operation of equation (34).

3.1 Consistency and convergence check of the present method for plane Poiseuille flow

We have performed some test calculations for the case of plane Poiseuille flow, i.e. a parabolic base velocity profile $U(y) = 1 - (y-1)^2$, $0 \leq y \leq 2$, for which various references can be found in the literature [8, 9, 10]. In this test, both walls are taken to be impermeable ($\beta = 0$). Furthermore, we focus on the value of $\mathrm{Re} = 10000$ for the Reynolds number as well as on a streamwise wavenumber of $\alpha = 1$. This is a slightly unstable mode with a maximum growth rate phase velocity of $c = 0.2375 + 0.0037i$.

In figure 5 we have plotted the convergence of the eigenvalue calculation for an equidistant knot point distribution of the sixth order spline base. It can be seen that the real as well as the imaginary part are obtained within 6 digits of accuracy by using 50 splines. The associated right eigenvectors are given in figure 6 as compared to the results of Thomas [8] who has used an eigth order finite difference scheme. An accurate representation of the imaginary part, which has small amplitude and high gradients, requires around 200 splines, whereas the real part can be obtained reasonably well with 50 splines.

4 Results

4.1 Recap of the inviscid analysis for a piecewise linear base profile

Since the perfectly permeable case ($\beta \to \infty$) corresponds to the problem of a piecewise linear wake-type flow (figure 3), which is known to be inviscidly unstable, our present problem of a porous wall was *a priori* expected to be also unstable in the inviscid approximation. The interesting question, however, was on which side of the spectrum of the porosity ($\beta \to 0+$ or $\beta \to \infty$) the stability limit would occur. As was deduced in section 2.1, the instability effectively takes place at infinitesimaly small values of porosity. This result is no longer true when viscosity is taken into account as can be seen in the following section.

Although the absence of viscosity is a rough assumption, let us consider the qualitative results obtained by this analysis which will be found to carry quite some resemblance to the numerically treated viscous case. The growth rate corresponding to different non dimensional porosity coefficients is plotted in figure 7 versus the non dimensional wave number. We retain the following characteristics:

- the flow is unstable for all positive β values;

- the growth rate increases with β toward an asymptotic value;
- the most unstable α slightly increases with β;
- for any finite β all the wave numbers are excited.

4.2 Viscous analysis of a turbulent base profile

We recall that the results of this section are based on a Reynolds-Tiedermann mean velocity profile at $\mathrm{Re}_\tau = 180$ (which corresponds quite closely to the low Reynolds numbers realized commonly in channel flow DNS and especially those including porous walls performed by the authors). For the numerical analysis we use 200 splines of order 6 whose knot points are distributed along the wall-normal coordinate according to the hyperbolic tangent mapping function given in appendix B.2. We have thus computed the most unstable eigenvalue of the general system (36), i.e. whose imaginary part $\Im(c)$ represents the growth rate of the disturbance, for a large number of values of the parameter pair of streamwise wavenumber and porosity (α, β).

A general view of the parametric function $\Im(c)(\alpha, \beta)$ is given in figure 8. As for the invisid case the growth rate increases with β up to an asymptotic value, also the most unstable α increases with β. On the other hand, not all the β values give rise to un unstable condition. In particular, from figure 9 it becomes obvious that a critical value of $\beta_c \approx 0.025$ exists below which all wave numbers are stable. When considering values of β larger than the critical value only part of the wave number spectrum is unstable due to viscous effects and no exponential tail is detected.

Figure 10 gives the neutral curve as well as α corresponding to the maximum growth rate for a given value of β. A high dependence on β is noted for both the curves, in contrast to the finding of the inviscid analysis. In particular, the upper wavenumber limit for stability at a given value of the porosity coefficient increases strongly with β so that a nearly horizontal neutral curve can be observed in figure 10 (b) and (c). At large values of porosity, the dependence levels off to an asymptotic value of the upper critical wavenumber of around 50. Similarly, the highest growth rate is obtained asymptotically at $\alpha \approx 18.5$.

As far as the eigenfunctions are concerned (figure 11) three values of β have been singled out. The first two (*case 1*: $\beta = 0.0039$; *case 2*: $\beta = 0.005$) correspond to values used in the DNS of the authors. The last one (*case 3*: $\beta = 0.36$) has been selected to study a high porosity case. The procedure to select the given eigenfunction has been the following: check for the α that gives the highest growth rate at a fixed β (solid curve of figure 10); for such an α we have determined the most unstable eigenvalue λ_{imax} and the corresponding eigenfunction $\vec{r}_{imax}$.

Since the eigenfunctions $\vec{r}_{imax}$ as such are somewhat difficult to interpret physically, we calculate the corresponding perturbation streamfunction,

$$\psi(x, y, t) = \{\Re(r_{imax}(y)) \cos(\alpha x - \alpha \Re(c) t) - \Im(r_{imax}(y)) \sin(\alpha x - \alpha \Re(c) t)\} \, e^{\Im(c) t}$$

which is given in figure 12. The most unstable mode takes obviously the shape of an array of spanwise vortices with the center biased towards the porous wall and a distorsion in the wall-normal direction. This shape is indeed similar to Tollmien-Schlichting waves although the underlying instability mechanism was seen to be distinct. As the porosity is increased, the center of the perturbation vortices approaches the lower wall, signifying the fact that the perturbations become more and more constrained to the vicinity of the porous surface itself.

5 Conclusions

Introduction of a porous wall destabilizes a turbulent-channel-type mean flow which is well-known to be linearly stable in the classical case of an impermeable wall. This instability is different from the viscous instability observed in wall-bounded shear flows (Tollmien-Schlichting instability)

inasmuch as it is basically a non-viscous mechanism closely related to wake-type flow instability as observed in free shear flows (Kelvin-Helmholtz instability). The fastest growing perturbations have the shape of alternating spanwise vortices which could be linked to the observations made in the authors' DNS of channel flow over porous walls. The next step in this study should be to clearly identify related structures in the flow fields obtained by non-linear simulation and compare their streamwise wavenumber to the above linear results.

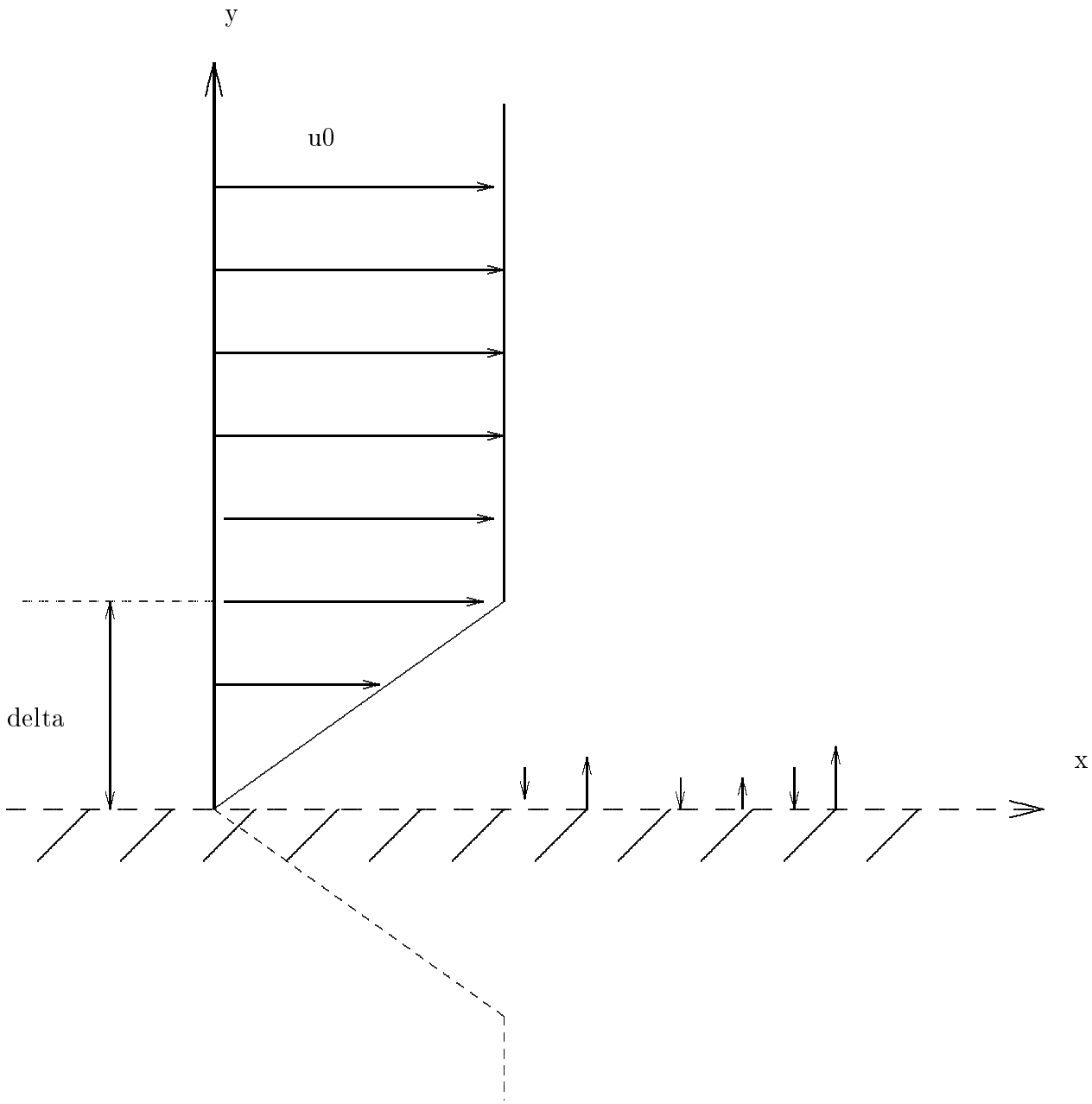

Figure 2: Schematic of the linear base profile considered in this section, indicating the wall-normal velocity at the surface for the permeable case as well as the shape of the streamwise perturbation of wavenumber α.

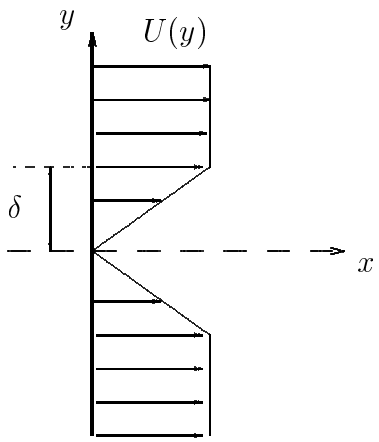

Figure 3: Schematic of the piecewise linear wake flow.

Part II

Model flow for streak instability

6 Introduction

Experimentally and numerically observed "bursting" phenomena of near-wall turbulence have been linked to an instability of the low- and high-speed streaks in past studies (e.g. the review in [11]). The question about the exact nature of such "bursting" events is of high relevance since they seem to play a key role in the regeneration cycle of wall turbulence. Jiménez and Pinelli [12] have recently shown in a series of numerical experiments that a removal of the streaks – by explicitely filtering in the near-wall region – eventually leads to a relaminarization of the flow. On the other hand, they showed in a particular "clean" environment (i.e. having damped outer turbulence) that the breakup of streaks effectively gives rise to new streamwise vortices. Although the exact mechanism of the instability of the streaks was not examined in that paper, the visualizations seem to suggest a spanwise bending or sinous mode to be responsable.

The issue of stability of the streaks in near-wall turbulence has been directly adressed by a number of authors in the past (e.g. [13, 14]). Only recently has a three-dimensional model flow been considered by Schoppa and Hussain [15]. These authors in fact performed temporarily evolving DNS of the specific base flow with prescribed perturbations and obtained some new results, namely confirming the dominance of a sinusoidal mode. We feel, however, that an analytic approach would be beneficial since – if successful – it can provide detailled insight into the mechanism of the respective instability.

mention: drag reduction/enhancement

We have thus embarked upon the linear stability analysis of a simple piecewise linear model of a streaky base flow (comprising a constant shear in the wall-normal direction and a spanwise "peak"-like streak distribution) which turns out to be already sufficiently intricate such as to deter pure analysis. As a consequence, in the present work we opt for a numerical solution of the discretized equations arising from linear stability analysis. This procedure of course allows for a more realistic base flow to be investigated.

In the following section we proceed by giving an outline of the stability analysis before presenting the numerical details in section 8. In section **??** we discuss the results of our calculations and draw some conclusions in section **??**.

7 Linear stability analysis

In this part of the present report, the considered three-dimensional flow will be described by the transport equations for the laplacian of the wall-normal velocity,

$$\partial_t(\nabla^2 v) \;=\; h_v \;+\; \frac{1}{\mathrm{Re}}\nabla^2(\nabla^2 v)\,, \qquad h_v = (\partial_{xx}+\partial_{zz})\,H_2 - \partial_{xy}H_1 - \partial_{yz}H_3\,, \tag{37}$$

where

$$H \;=\; \vec{\omega} \;\times\; \vec{v} \;-\; \frac{1}{2}\nabla(|\vec{u}^2|)\,, \tag{38}$$

the equation for the wall-normal vorticity ($\eta \equiv \partial_z u - \partial_x w$),

$$\partial_t(\eta) \;=\; h_g \;+\; \frac{1}{\mathrm{Re}}\nabla^2(\eta)\,, \qquad h_g = \partial_z H_1 - \partial_x H_3\,, \tag{39}$$

and the continuity equation:

$$\nabla\cdot\vec{v} \;=\; 0\,. \tag{40}$$

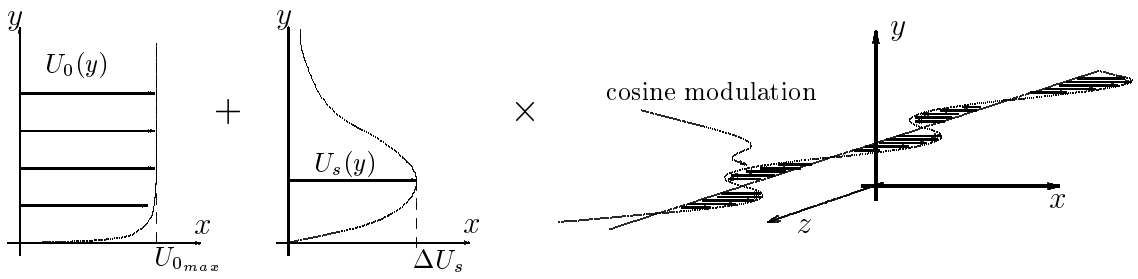

Figure 4: Schematic of the base flow velocity field consisting of a streamwise velocity profile $U(y)$ and a spanwise cosine-modulated streak model of a Gaussian type shape in wall-normal direction.

The base flow that we will consider for the streak instability is unidirectional and consists of a turbulent velocity profile $U_0(y)$ (Reynolds-Tiedermann) as used in part I of this report upon which a 'streak' velocity $U_s(y)$ of gaussian form is superimposed which in turn is modulated in spanwise direction by a cosine function with the wavenumber γ, viz.

$$U(y,z) \;=\; U_0(y) \;+\; U_s(y)\cdot\cos(\gamma\, z) \quad , \tag{41}$$

where $U_0(y)$ is given by equation (27) and the 'streak' contribution $U_s(y)$ reads

$$U_s(y) \;=\; \Delta U_s \frac{\sqrt{\sigma} y \exp(-\sigma y^2)}{\exp(-1/2)/\sqrt{2}} \quad . \tag{42}$$

The parameter ΔU_s gives the amplitude of the streak while the scaling factor σ defines the location of the maximum with respect to the wall ($y_{max} = 1/\sqrt{2\,\sigma}$). This model of a streak arrangement (see figure 4 for a schematic representation) is in fact quite similar to the one employed by Schoppa and Hussein [15] in their analysis (for correspondance, $\sigma\,\sqrt{h} = 1/(2\times 30^2)$ needs to be chosen).

After introducing the usual decomposition of the flow field into small perturbations and the contribution from the base flow,

$$\begin{aligned} u(x,y,z,t) &= U(y,z) \;+\; u'(x,y,z,t) \\ v(x,y,z,t) &= v'(x,y,z,t) \\ w(x,y,z,t) &= w'(x,y,z,t)\,, \end{aligned} \tag{43}$$

and linearizing, the system of equations takes the following form:

$$\left(\partial_t + U\partial_x - \frac{1}{\mathrm{Re}}\nabla^2\right)\nabla^2 v - \left(\partial_{yy}U - \partial_{zz}U\right)\partial_x v - 2\left(\partial_z U\right)\partial_x\left(\partial_y w - \partial_z v\right)$$
$$-2\left(\partial_{yz}U\right)\partial_x w \;=\; 0 \tag{44}$$

$$\left(\partial_t + U\partial_x - \frac{1}{\mathrm{Re}}\nabla^2\right)\eta - \left(\partial_z U\right)\partial_y v + \left(\partial_y U\right)\partial_z v + \left(\partial_y\partial_z U\right)v + \left(\partial_{zz}U\right)w \;=\; 0 \tag{45}$$

$$\partial_x u + \partial_y v + \partial_z w \;=\; 0 \tag{46}$$

$$\partial_z u - \partial_x w \;=\; \eta \quad , \tag{47}$$

where the primes indicating fluctuations have been dropped. In the following, we will treat normal mode solutions of the form

$$\begin{pmatrix} u \\ v \\ w \\ \eta \end{pmatrix}(x,y,z,t) \;=\; \begin{pmatrix} u \\ v \\ w \\ \eta \end{pmatrix}(y,z)\cdot \mathrm{e}^{i\alpha(x-ct)} \quad . \tag{48}$$

Furthermore, the variables will be expanded into some sine and cosine series in the spanwise direction. According to the choice of combined odd and even trigonometric polynomials three general 'modes' of solutions can be distinguished:

I fundamental sinusoidal mode

$$u(y,z) = \sum_{n=1}^{\infty} u_n(y)\ \sin(\gamma n z)\,, \qquad v(y,z) = \sum_{n=1}^{\infty} v_n(y)\ \sin(\gamma n z)\,,$$
$$w(y,z) = \sum_{n=0}^{\infty} w_n(y)\ \cos(\gamma n z)\,, \qquad \eta(y,z) = \sum_{n=0}^{\infty} \eta_n(y)\ \cos(\gamma n z)\,. \tag{49}$$

II varicose mode

$$u(y,z) = \sum_{n=0}^{\infty} u_n(y)\ \cos(\gamma n z)\,, \qquad v(y,z) = \sum_{n=0}^{\infty} v_n(y)\ \cos(\gamma n z)\,,$$
$$w(y,z) = \sum_{n=1}^{\infty} w_n(y)\ \sin(\gamma n z)\,, \qquad \eta(y,z) = \sum_{n=1}^{\infty} \eta_n(y)\ \sin(\gamma n z)\,. \tag{50}$$

III subharmonic mode

$$u(y,z) = \sum_{n=0}^{\infty} u_n(y)\ \sin(\gamma (n+\frac{1}{2}) z)\,, \qquad v(y,z) = \sum_{n=0}^{\infty} v_n(y)\ \sin(\gamma (n+\frac{1}{2}) z)\,,$$
$$w(y,z) = \sum_{n=0}^{\infty} w_n(y)\ \cos(\gamma (n+\frac{1}{2}) z)\,, \qquad \eta(y,z) = \sum_{n=0}^{\infty} \eta_n(y)\ \cos(\gamma (n+\frac{1}{2}) z)\,. \tag{51}$$

The solutions of the form (49), (50) and (51) together with the chosen base profile (41), when substituted into equations (44) to (47), give rise to a system of linear ordinary differential equations containing the above infinite series. In order for the relations to be generally satisfied, the matching coefficients of each member of the series need to be zero simultaneously. This results in a set of equations for each mode n of the spanwise expansion, where we note a coupling between n and its direct neighbours $n-1$ and $n+1$ through the spanwise dependence of the base profile (41). These modal equations are given in appendix C.2, a MAPLE routine to derive them from the basic equations is listed in appendix D.1.

8 Numerical procedure

In the numerical approach, the infinite series are replaced by truncated series up to $n = N_z$ spanwise modes. As in part I, section 3, we apply a Galerkin MWR to the stability equations (59)–(75), resorting to N_s b-splines of order 6 as the expansion functions in the wall-normal direction y.

The evaluation of the involved integrals (see appendix C.3 for details) leads to a large, coupled system of algebraic equations, $A \cdot \hat{x} = c \cdot B \cdot \hat{x}$, which is of order $N_s \cdot (N_z + 1 + N_z)$ (or $N_s \cdot (N_z + 1) \cdot 2$ in the case of the subharmonic mode solution). The solution vector $\hat{x}$ in spline space contains the coefficients of the wall-normal velocity and the normal vorticity for each spanwise mode and each discrete wall-normal location. The structure of the matrix A is block-tridiagonal in each quadrant, wheras the matrix B is of block mono-diagonal structure. Each block of size $N_s \cdot N_s$ is of $(2k-1)$-diagonal structure like the system discussed in part I of the present report. The reader is referred to the figure 15 for a more detailled description of the structure of the system.

References

[1] G.K. Batchelor. *An introduction to fluid dynamics.* Cambridge University Press, 1967.

[2] P. Koumoutsakos. Active control of turbulent channel flow. *CTR Res. Briefs*, pages 289–297, 1997.

[3] C. Wagner and R. Friedrich. On the turbulence structure in solid and permeable pipes. TSF 11, Grenoble, France, 1997.

[4] W.C. Reynolds and W.G. Tiedermann. Stability of turbulent channel flow, with application to Malkus's theory. *J. Fluid Mech.*, 27:253–272, 1967.

[5] C. Canuto, M.Y. Hussaini, A. Quarteroni, and T.A. Zang. *Spectral methods in fluid dynamics.* Springer, 1988.

[6] Available free on the following site:. `ftp.hensa.ac.uk\netlib`.

[7] J. Mizushima. private communication.

[8] L.H. Thomas. The stability of plane Poiseuille flow. *Phys. Review*, 91(4):780–791, 1953.

[9] S.A. Orszag. Accurate solution of the Orr-Sommerfeld equation. *J. Fluid Mech.*, 50:689–703, 1971.

[10] P.G. Drazin and W.H. Reid. *Hydrodynamic stability.* Cambridge University Press, 1981.

[11] R.F. Blackwelder. The eddy structure in bounded shear flows. Technical Report 786, AGARD, 1992.

[12] J. Jiménez and A. Pinelli. The autonomous cycle of near-wall turbulence. *J. Fluid Mech.*, 389:335–359, 1999.

[13] J. Jiménez and P. Moin. The minimal flow unit in near-wall turbulence. *J. Fluid Mech.*, 225:213–240, 1991.

[14] J.M. Hamilton, J. Kim, and F. Waleffe. Regeneration mechanisms of near-wall turbulence structures. *J. Fluid Mech.*, 287:317–348, 1995.

[15] W. Schoppa and F. Hussain. Genesis and dynamics of coherent structures in near-wall turbulence: a new look. In *Self-sustaining mechanisms of wall turbulence*, pages 385–422. R.L. Panton, 1997.

[16] K.M. Butler and B.F. Farrell. Optimal perturbations and streak spacing in wall-bounded turbulent shear flow. *Phys. Fluids A*, 5(3):774–777, 1993.

[17] A.G. Kravchenko, P. Moin, and R. Moser. Zonal embedded grids for numerical simulations of wall-bounded turbulent flows. *J. Comp. Physics*, 127:412–423, 1996.

[18] L.L. Schumaker. *Spline functions: basic theory.* J. Wiley, 1981.

[19] C. de Boor. *A practical Guide to Splines.* Springer, 1978.

[20] M. Abramowitz and I.A. Stegun. *Handbook of mathematical functions.* Dover, 1964.

Figures of part I

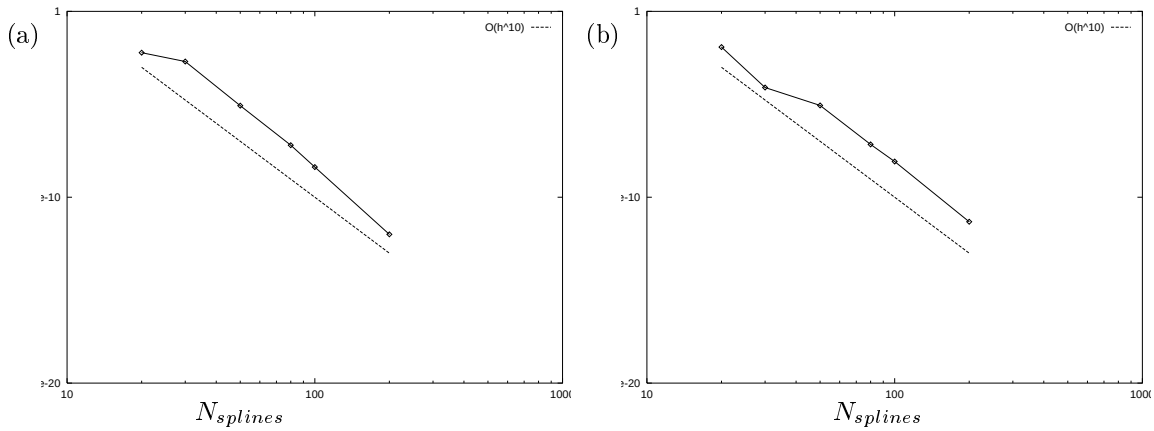

Figure 5: Convergence check of the most unstable eigenvalue calculation ($\lambda_{imax} = 0.237526 + 0.373967e^{-2}i$) in the case of plane Poiseuille flow at $\alpha = 1$ and Re $= 10000$. The error is calculated relative to our numerical value at $N_{splines} = 300$. (a) real part, (b) imaginary part.

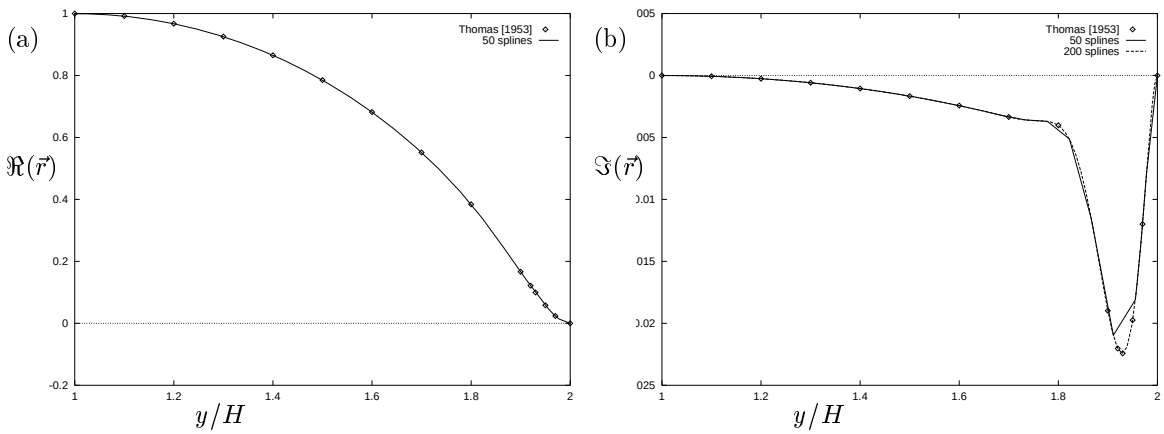

Figure 6: Eigenvector $\vec{r}_{imax}$ associated with the most unstable eigenvalue λ_{imax} of the plane Poiseuille flow stability problem at $\alpha = 1$, Re $= 10000$. Comparison with numerical results published by Thomas [8]. (a) real part, (b) imaginary part.

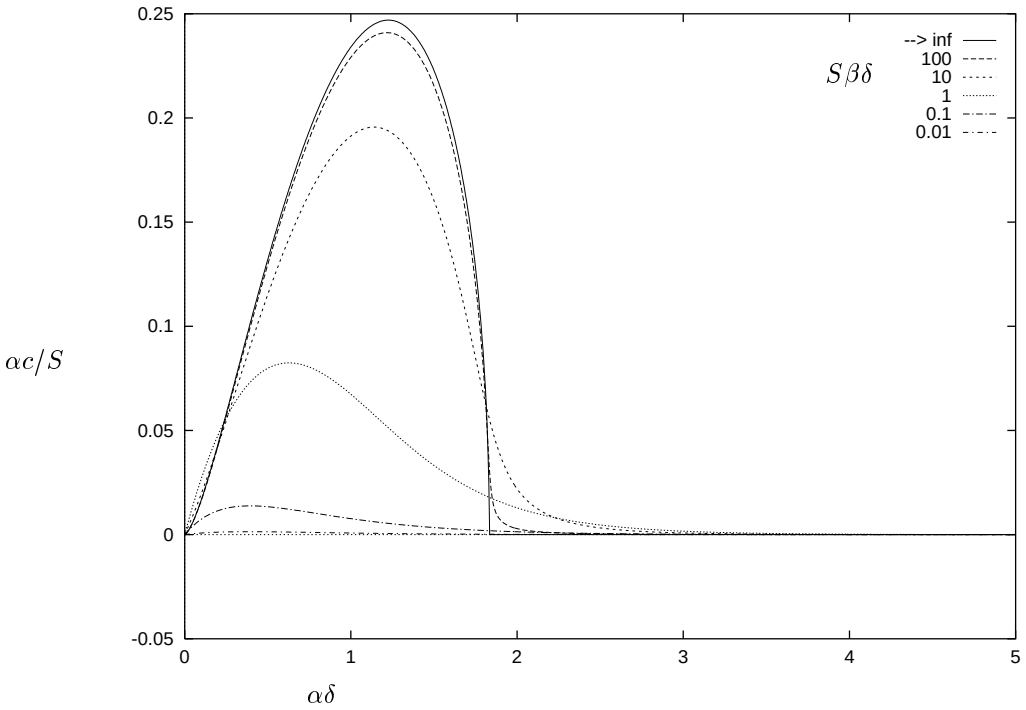

Figure 7: Growth rate vs. wave number α in the case of piecewise linear base flow: δ is the height of the shear region; β refers to Darcy's coefficient and S is the shear rate

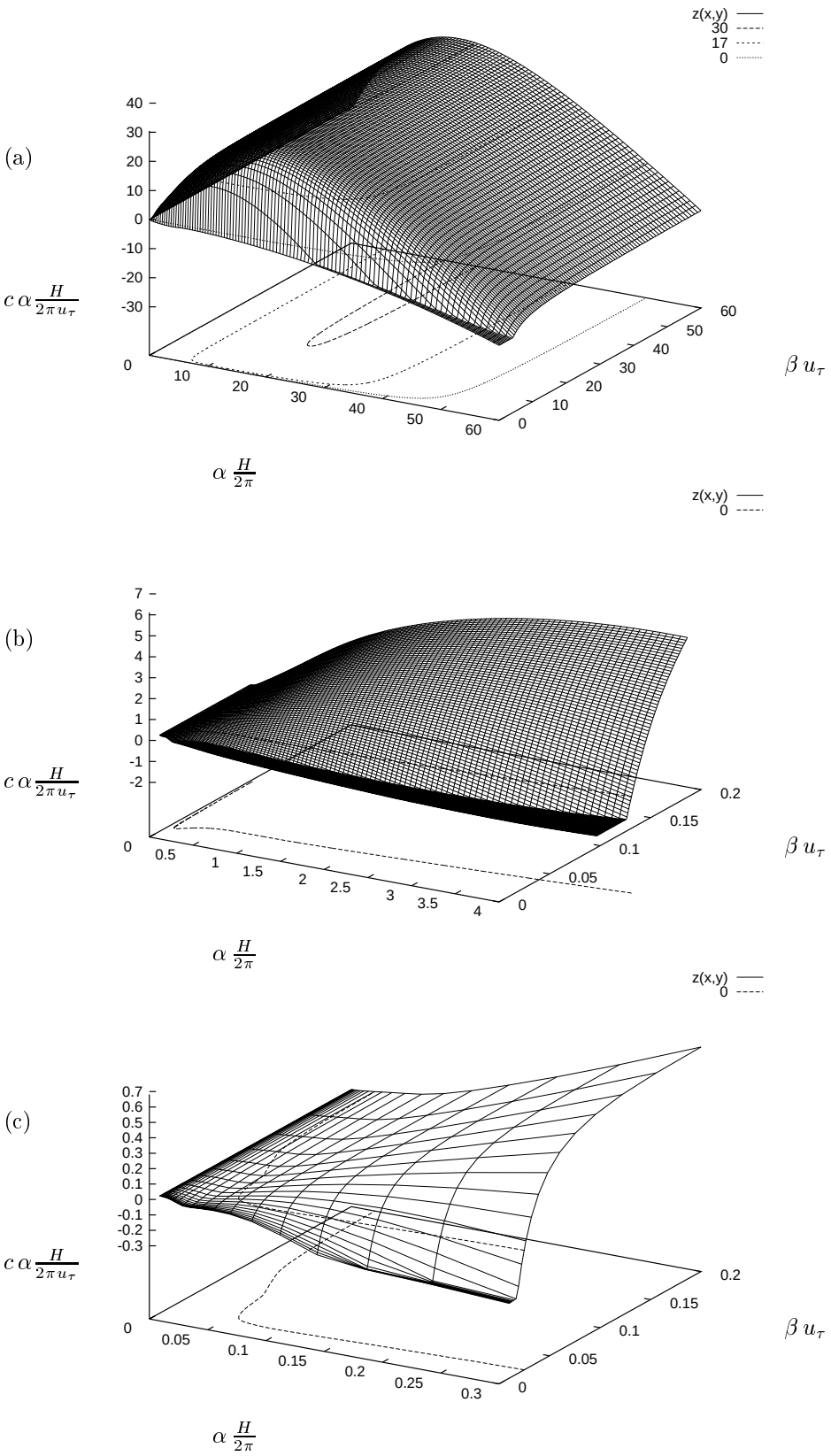

Figure 8: Temporal growth rate c of perturbation as a function of streamwise wavenumber α, and the porosity constant β. a) global view b) small scale view c) close-up of origin. The isoline on the surface and on the bottom plane indicates the region of the stability limit.

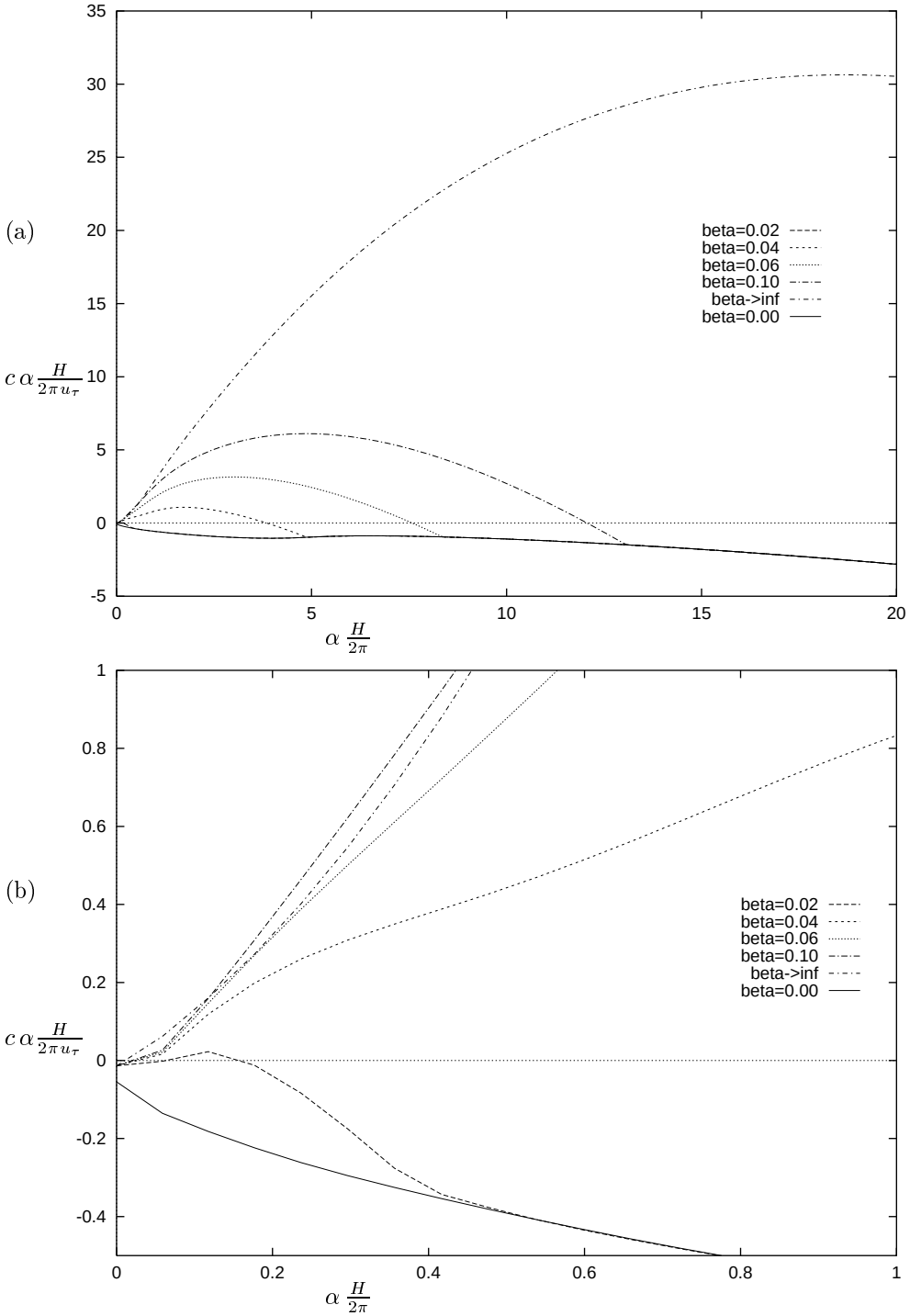

Figure 9: Temporal growth rate c of perturbation as a function of streamwise wavenumber α, parametrized by the porosity constant β. (a) global view, (b) close-up.

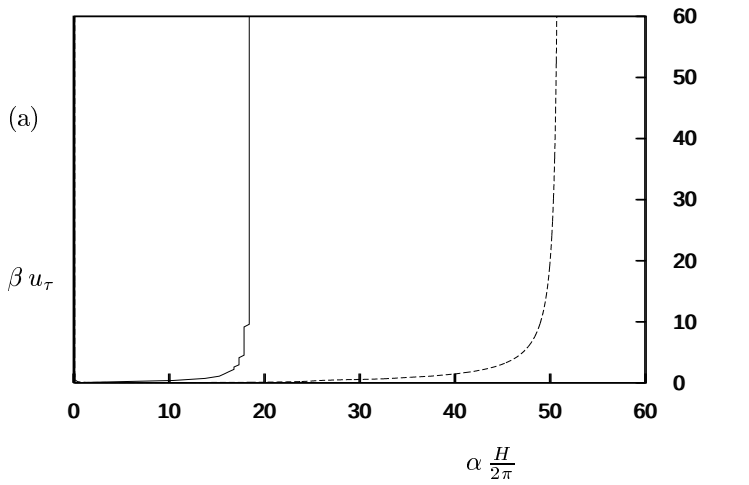

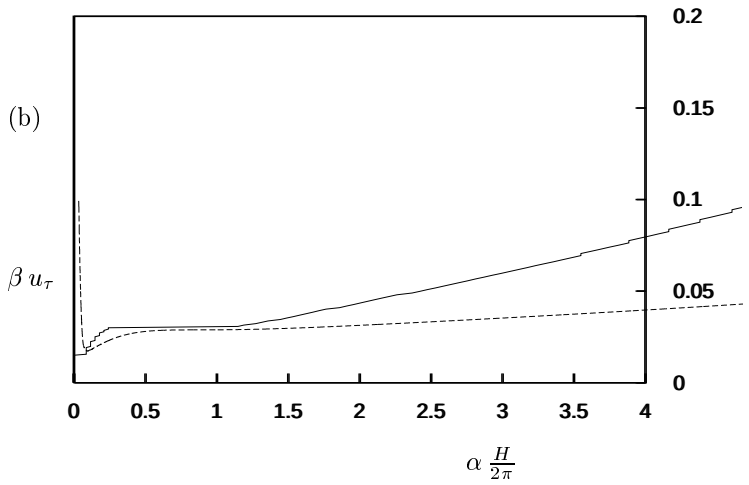

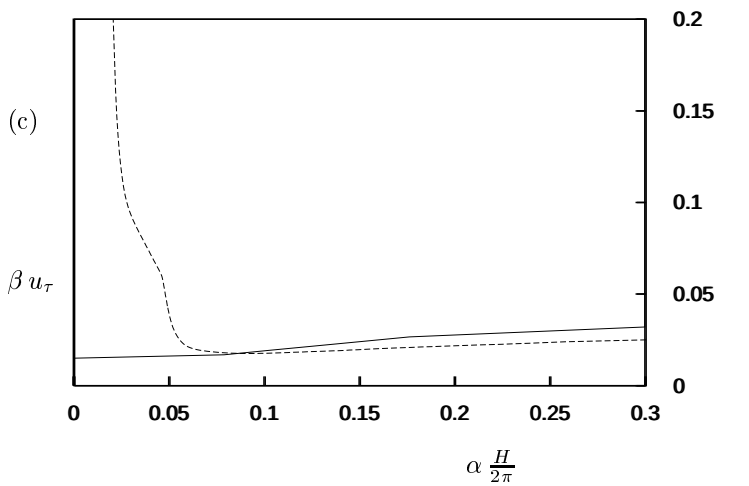

Figure 10: Isolines indicating: - - the limit of the unstable region, — the location of the most unstable wavenumber. a) global view b) small scale view (c) close-up of origin.

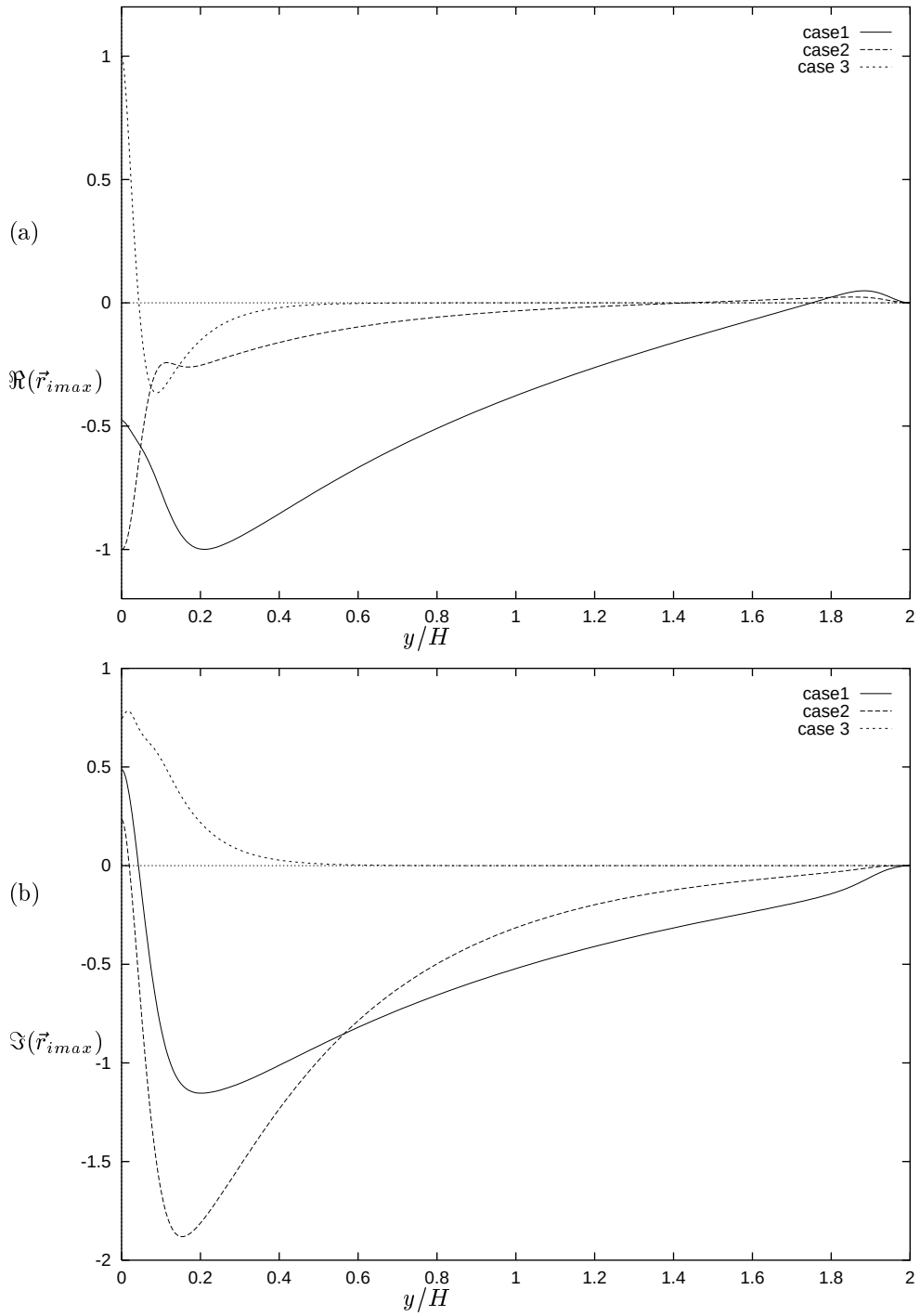

Figure 11: Eigenvectors $\vec{r}_{imax}$ associated with the most unstable eigenvalue λ_{imax} for the case of a plane turbulent channel flow (Reynolds-Tiedermann velocity profile) at $\mathrm{Re}_\tau = 180$ for successively higher values of porosity β, in each case considering the streamwise wavenumber α for which the temporal growth rate of the disturbance takes a maximum. The values are normalized such that the maximum absolute value of the real part is unity. (a) real part, (b) imaginary part.

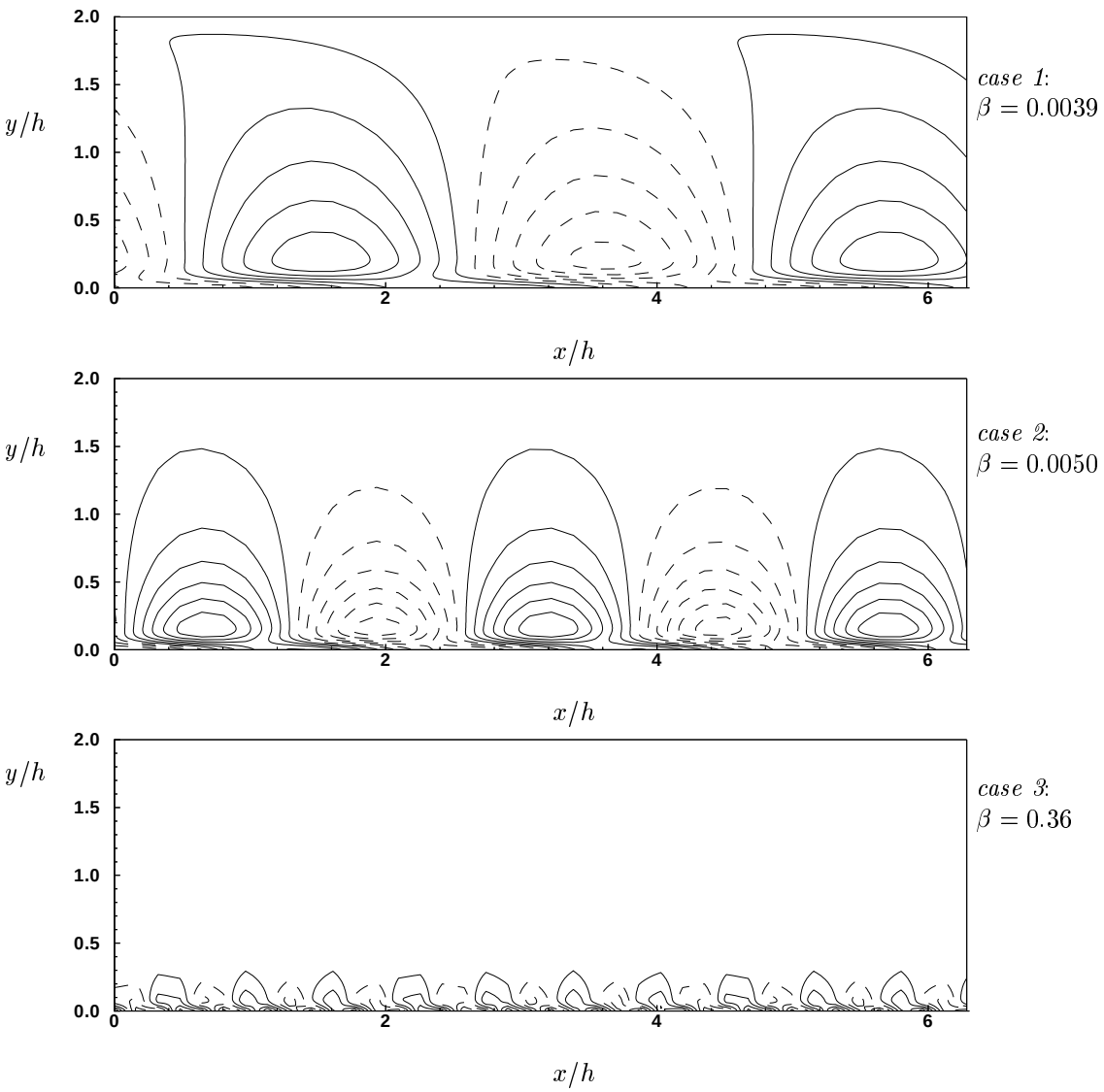

Figure 12: Perturbation streamfunctions associated with the most unstable eigenvalue at wavenumber α giving maximum growth rate for three different values of porosity at $t = 0$. Isolines are from -2 to 2 with increments of .25; dashed lines indicating negative values

A On the Reynolds–Tiederman velocity profile in a turbulent channel

The Reynolds–Tiederman profile of a mean velocity in a turbulent channel flow is expressed as [4]

$$\frac{\mathrm{d}U}{\mathrm{d}y} = -\frac{Ry}{1+\nu_t(y)} \quad (-1 < y < 1), \tag{1}$$

$$\nu_t(y) = \tfrac{1}{2}\left\{1 + \left[\frac{KR}{3}(1-y^2)(1+2y^2)\left(1-\exp\left(-\frac{(1-|y|)R}{A}\right)\right)\right]^2\right\}^{\frac{1}{2}} - \tfrac{1}{2},$$

where

$$R = \frac{u_\tau h}{\nu}$$

is a Reynolds number based on friction velocity u_τ and channel half-width h. For $R = 180$ the values, $K = 0.525$ and $A = 37$, were used in Butler and Farell [16], and here we use the same values for *all* Reynolds numbers below. In equation (1) y has been normalized by h, and the profile is symmetrized about the center of a channel, $y = 0$. The figure shown below is the comparison of velocity profiles between equation (1) and direct numerical simulations at three Reynolds numbers $R = 150, 395$ and 590.

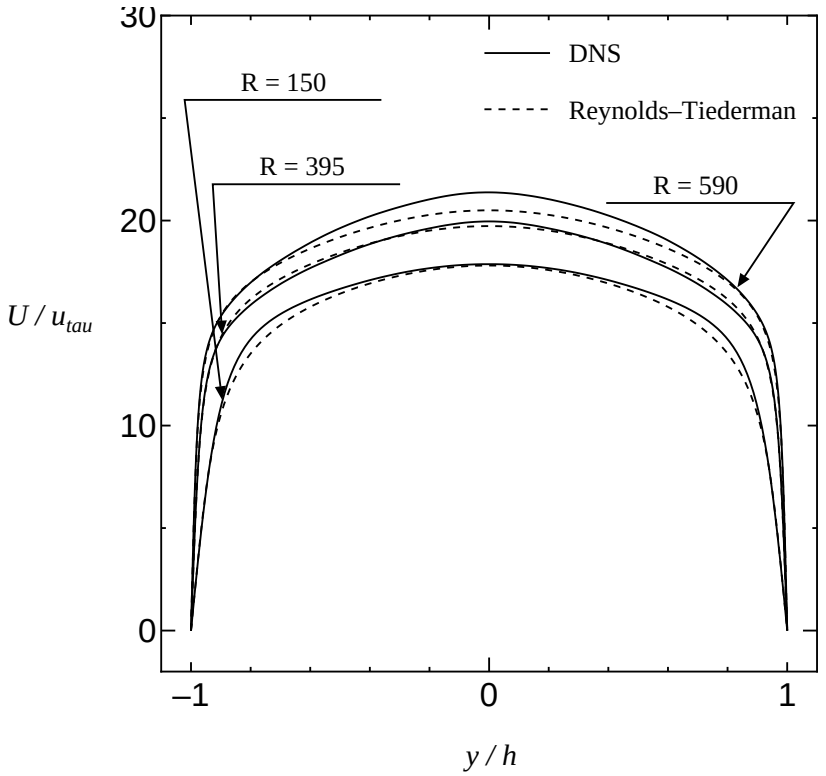

Figure 13: Comparison of velocity profiles between Reynolds–Tiederman's empirical equation (1) and direct numerical simulations done by Kuroda & Kasagi [?] for $R = 150$, and by Mansour, Moser & Kim [?] for $R = 395$, and 590.

$\mathrm{d}U/\mathrm{d}y$ is apparently continous at $y = 0$, while $\mathrm{d}\nu_t/\mathrm{d}y$ is discontinous at $y = 0$. However, we consider the second derivative of U itself to have the expression as

$$\frac{\mathrm{d}^2 U}{\mathrm{d}y^2} = -R\frac{1 + \nu_t - y\dfrac{\mathrm{d}\nu_t}{\mathrm{d}y}}{(1 + \nu_t)^2},$$

which is continous at $y = 0$. Thus, the velocity profile defined by equation (1) has the continuity at least up to the second-order derivative, which appears in the Orr–Sommerfeld equation.

B B-spline expansion

B-spline functions have been used in fluid mechanics problems by various authors in the past [17, ?]. The advantages of using b-spline functions for the projection of the respective flow variables are roughly the following:

- local support of each spline gives rise to banded matrices,
- high continuity at knot points,
- flexibility of boundary treatment,
- free choice of grid stretching.

On the other hand these points are partially offset by a somewhat intricate coding in practice.

B.1 The present spline base

Classic textbooks [18, 19] give the mathematical background on b-splines, which are here recalled to be piecewise polynomial functions that can be most conveniently defined by the following recursion formula:

$$B_j^k(x) = \frac{(x - t_{j-k-1})}{(t_{j-1} - t_{j-k-1})} B_j - 1^{k-1}(x) \; + \; \frac{(t_j - x)}{(t_j - t_{j-k})} B_j^{k-1}(x) \quad j = 1 \ldots N \quad , \tag{52}$$

where $B_j^k(x)$ denotes the j-th b-spline of order k and $t = \{t1, \ldots, t_{N+k}\}$ is a set of knot points which will determine completely the desired spline base. We note that a spline function of order k as defined in this context consists actually of polynomials of degree $k-1$. The number of necessary points for the construction of N splines of order k is $N+k$ since each spline has a support of $k+1$ knots.

Among the various possibilities, we use the technique of multiple knots at the extrema [19] for our present purposes. As can be seen on figure B.1, k identical knot point locations are accumulated at each boundary which gives rise to the particular spline base seen in this figure, simplifying the treatment of boundary conditons as will become obvious below.

A spline expansion of a variable $f(x)$ in terms of b-splines B_i^k,

$$f(x) \; = \; \sum_{i=1}^{N} \hat{f}_i \cdot B_i^k(x) \quad , \tag{53}$$

necessitates a transformation of N discrete functional values $f(x_j)$, $j = \{1 \ldots N\}$ to spline coefficients $\hat{f}_j$, $j = \{1 \ldots N\}$. As collocation points x_j for this transformation, we choose the $N + (2-k)$ non-coinciding knot points out of the set $\{t_l\}$ which we supplement by $(k-2)$ additional points in the intervals $[t_k, t_{k+1}]$ and $[t_{N-k-1}, t_{N-k}]$ in order to obtain a closed and well-posed system of order N. Specifically in the case of splines of order $k = 6$, which will be employed throughout the present work, we choose the 4 additional points to be located at $x_{3,4} = \{(t_6 + t_7)/2, 3(t_7 - t_6)/4 + t_6\}$ and $x_{N-2,N_1} = \{t_{N-7} + (t_{N-6} - t_{N-7})/4, (t_{N-6} + t_{N-7})/2\}$ (see figure B.1).

B.2 Analytical grid mapping

In order to increase the spatial resolution in the regions of high gradients we accumulate knot points near the wall locations at the extremas. The advantage of an analytical mapping function is that in a collocation method the chain rule can be used to obtain gradients of flow variables, effectuating numerical differentiation simply on equidistant mesh. This fact cannot be exploited

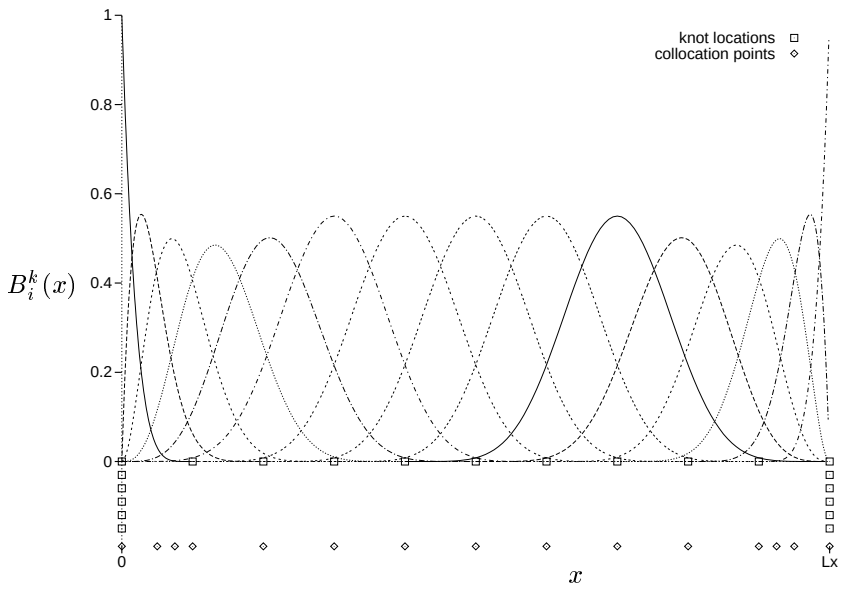

Figure 14: Example of a spline base consisting of 15 b-splines of order $k = 6$ constructed on 21 equidistant knots with multiplicty 6 on the extremas. Also indicated are the corresponding locations of the collocation points for variable transformation.

in the Galerkin framework, where the system matrices need to be constructed in non-equidistant space. The following mapping function is, however, used to define the locations of our knot points.

We use a hyperbolic tangent function $g(t(\xi))$ to map an equidistant mesh of knot points $t(\xi)$ onto a non-equidistant set $t(x)$:

$$g(t(\xi)) \;=\; 1 + \frac{\tanh(2\alpha(t(\xi)-1)\pi)}{\tanh(2\alpha\pi)} \qquad 0 \le t(\xi) \le 2 \quad . \tag{54}$$

The parameter α being set to 0.3, this function gives a stretching ratio $\Delta x_{max}/\Delta x_{min} \approx 11$.

B.3 Galerkin procedure

Inserting the b-spline expansion (53) into the system of equations given by the method of weighted residuals (33) leads to the following system of algebraic equations involving integrals of double

and triple products of b-splines:

$$
\begin{aligned}
&-\frac{1}{i\alpha\mathrm{Re}} \sum_j \hat{\psi}_j \int_0^{L_y} B_j^{(iv)}(y)\, B_i(y)\, \mathrm{d}y \\
&- \sum_k \sum_j \hat{U}_k\, \hat{\psi}_j \int_0^{L_y} B_k''(y)\, B_j(y)\, B_i(y)\, \mathrm{d}y \\
&+ \sum_k \sum_j \hat{U}_k\, \hat{\psi}_j \int_0^{L_y} B_k(y)\, B_j''(y)\, B_i(y)\, \mathrm{d}y \\
&- \alpha^2 \sum_k \sum_j \hat{U}_k\, \hat{\psi}_j \int_0^{L_y} B_k(y)\, B_j(y)\, B_i(y)\, \mathrm{d}y \\
&+ \left(\frac{2\alpha}{i\mathrm{Re}} - c\right) \sum_j \hat{\psi}_j \int_0^{L_y} B_j''(y)\, B_i(y)\, \mathrm{d}y \\
&- \left(c\alpha^2 - \frac{\alpha^3}{i\mathrm{Re}}\right) \sum_j \hat{\psi}_j \int_0^{L_y} B_j(y)\, B_i(y)\, \mathrm{d}y \;=\; 0 \quad .
\end{aligned}
\tag{55}
$$

Since the coefficients of the base profile $\hat{U}_k$ are known values, the above expressions can be reduced to two indices. Let us define the following square N by N matrices whose entries are:

$$
\begin{aligned}
M_{40\,ij} &= \int_0^{L_y} B_j^{(iv)}(y)\, B_i(y)\, \mathrm{d}y \\
\widetilde{M}_{ij}(\hat{U}) &= \sum_k \hat{U}_k \int_0^{L_y} B_k''(y)\, B_j(y)\, B_i(y)\, \mathrm{d}y \\
\widetilde{K}_{ij}(\hat{U}) &= \sum_k \hat{U}_k \int_0^{L_y} B_k(y)\, B_j''(y)\, B_i(y)\, \mathrm{d}y \\
\widetilde{\widetilde{M}}_{ij}(\hat{U}) &= \sum_k \hat{U}_k \int_0^{L_y} B_k(y)\, B_j(y)\, B_i(y)\, \mathrm{d}y \\
K_{ij} &= \int_0^{L_y} B_j''(y)\, B_i(y)\, \mathrm{d}y \\
M_{ij} &= \int_0^{L_y} B_j(y)\, B_i(y)\, \mathrm{d}y \quad ,
\end{aligned}
\tag{56}
$$

which have a $(2N-1)$-banded structure due to the local support of the splines. The evaluation of the above double and triple integrals can be done exactly (up to machine accuracy) by Gauss quadrature using 8 Gauss-Legendre points [20, p.916]. Inserting the definitions (56) into the preceding equation (55) leads to the formula (35) given in the main text.

B.4 Treatment of boundary conditions

The boundary conditions stated in section 2.2 are discretized by using a simple spline collocation method, i.e. requiring the respective condition to hold exactly for the spline coefficients involved. Inserting the b-spline expansion (53) directly into the differential expressions (31) and (32) leads to the folowing relations:

continuity, no-slip

$$
\sum_j \hat{\psi}_j\, B_j'(y = y_w) \;=\; 0 \qquad\qquad y_w = \{0, 2\} \quad , \tag{57}
$$

impermeability/porosity

$$\sum_j \hat{\psi}_j \, B_j(y=0) \quad = \quad 0$$

$$\left(\beta \sum_k \hat{U}_k \, B'_k(y=0) - i\alpha \right) \sum_j \hat{\psi}_j \, B_j(y=0)$$

$$+ \frac{\beta}{i\alpha \mathrm{Re}} \sum_j \hat{\psi}_j \, B'''_j(y=0) \quad = \quad 0 \quad . \tag{58}$$

The above conditions only involve few coefficients (at the extremas: 1 b-spline value, 2 first derivative values, 4 third derivative contributions etc. are non-zero) thus giving rise to few entries into the respective matrices. We simply replace the first two and the last two equations of the system matrices A and B (see equation (36)) by the entries stemming from the above conditions. More specifically, matrix B will have those lines set to zero due to the homogeneity of the expressions (57) and (58).

B.5 Gauss elimination of boundary values

The method suggested by Mizushima [7] consists of performing 4 sweeps of Gauss elimination on the system (36) such that the first and last two rows of matrix A have zero entries in lines 3 thru $(N-2)$ by using elements $(1,1)$, $(2,2)$, $(N-1,N-1)$ and (N,N) as the respective pivots. The first and last two rows are now exchanged between matrix A and B (which is appropriate, since corresponding entries in B are still all zero) and the same elimination is performed once more on matrix B. As a result, the four eigenvalues with index $\{1,2,N-1,N\}$ are effectively decoupled from the remaining ones and the reduced system of size $(N-4) \times (N-4)$ can be subjected to the eigensystem analysis.

C Details of the streak instability problem

C.1 Linear stability equations

Substituting the series expansions for the independent variables and combining the repsective trigonometric functions where possible gives rise to a set of ODEs. In the following, as an example, we reproduce – with respect to the sinusoidal mode – the normal velocity equation:

$$
\begin{aligned}
&\sum_{n=1}^{\infty} -2\,\frac{\sin(\gamma\,nz)v_n(y)\gamma^2n^2\alpha^2}{\mathrm{Re}} + \sum_{n=1}^{\infty} 1/2\,i\alpha\,U_s(y)\left(\frac{d^2}{dy^2}v_n(y)\right)\sin(\gamma\,nz-\gamma\,z)\\
&\quad+\sum_{n=1}^{\infty} i\,v_n(y)\sin(\gamma\,nz)\gamma^2n^2\alpha\,c+\sum_{n=0}^{\infty} iU_s(y)\gamma\,\alpha\,\left(\frac{d}{dy}w_n(y)\right)\sin(\gamma\,nz+\gamma\,z)\\
&\quad+\sum_{n=1}^{\infty} -1/2\,i\alpha^3U_s(y)v_n(y)\sin(\gamma\,nz+\gamma\,z)+\sum_{n=1}^{\infty} -i\left(\frac{d^2}{dy^2}v_n(y)\right)\sin(\gamma\,nz)\alpha\,c\\
&\quad+\sum_{n=1}^{\infty} i\sin(\gamma\,nz)\alpha\;U_0(y)\frac{d^2}{dy^2}v_n(y)+\sum_{n=1}^{\infty} -1/2\,i\alpha\,U_s(y)v_n(y)\gamma^2n^2\sin(\gamma\,nz-\gamma\,z)\\
&\quad+\sum_{n=1}^{\infty} -\frac{\sin(\gamma\,nz)v_n(y)\alpha^4}{\mathrm{Re}}+\sum_{n=1}^{\infty} -iU_s(y)\gamma^2\alpha\,v_n(y)n\sin(\gamma\,nz+\gamma\,z)\\
&\quad+\sum_{n=1}^{\infty} -iU_s(y)\gamma^2\alpha\,v_n(y)n\sin(\gamma\,z-\gamma\,nz)+\sum_{n=1}^{\infty} 1/2\,i\alpha\,U_s(y)\left(\frac{d^2}{dy^2}v_n(y)\right)\sin(\gamma\,nz+\gamma\,z)\\
&\quad+\sum_{n=1}^{\infty} i\,v_n(y)\sin(\gamma\,nz)\alpha^3c+\sum_{n=1}^{\infty} -1/2\,i\alpha^3U_s(y)v_n(y)\sin(\gamma\,nz-\gamma\,z)\\
&\quad+\sum_{n=1}^{\infty} -1/2\,i\alpha\,U_s(y)v_n(y)\gamma^2n^2\sin(\gamma\,nz+\gamma\,z)+\sum_{n=0}^{\infty} i\left(\frac{d}{dy}U_s(y)\right)\gamma\,w_n(y)\alpha\;\sin(\gamma\,z-\gamma\,nz)\\
&\quad+\sum_{n=0}^{\infty} i\left(\frac{d}{dy}U_s(y)\right)\gamma\,w_n(y)\alpha\;\sin(\gamma\,nz+\gamma\,z)+\sum_{n=1}^{\infty} -i\sin(\gamma\,nz)\alpha\;U_0(y)v_n(y)\gamma^2n^2\\
&\quad+\sum_{n=0}^{\infty} iU_s(y)\gamma\,\alpha\,\left(\frac{d}{dy}w_n(y)\right)\sin(\gamma\,z-\gamma\,nz)+\sum_{n=1}^{\infty} -1/2\,iv_n(y)\alpha\,\left(\frac{d^2}{dy^2}U_s(y)\right)\sin(\gamma\,nz-\gamma\,z)\\
&\quad+\sum_{n=1}^{\infty} -1/2\,iv_n(y)\alpha\,U_s(y)\gamma^2\sin(\gamma\,nz+\gamma\,z)+\sum_{n=1}^{\infty} -1/2\,iv_n(y)\alpha\,U_s(y)\gamma^2\sin(\gamma\,nz-\gamma\,z)\\
&\quad+\sum_{n=1}^{\infty} -1/2\,iv_n(y)\alpha\,\left(\frac{d^2}{dy^2}U_s(y)\right)\sin(\gamma\,nz+\gamma\,z)+\sum_{n=1}^{\infty} -i\sin(\gamma\,nz)\alpha^3\,U_0(y)v_n(y)\\
&\quad+\sum_{n=1}^{\infty} -iv_n(y)\sin(\gamma\,nz)\alpha\,\frac{d^2}{dy^2}U_0(y)+\sum_{n=1}^{\infty} -\frac{\left(\frac{d^4}{dy^4}v_n(y)\right)\sin(\gamma\,nz)}{\mathrm{Re}}\\
&\quad+\sum_{n=1}^{\infty} 2\,\frac{\sin(\gamma\,nz)\left(\frac{d^2}{dy^2}v_n(y)\right)\alpha^2}{\mathrm{Re}}+\sum_{n=1}^{\infty} -\frac{\sin(\gamma\,nz)v_n(y)\gamma^4n^4}{\mathrm{Re}}\\
&\quad+\sum_{n=1}^{\infty} 2\,\frac{\sin(\gamma\,nz)\left(\frac{d^2}{dy^2}v_n(y)\right)\gamma^2n^2}{\mathrm{Re}} \;=\; 0
\end{aligned}
$$

and the normal vorticity equation:

$$\begin{aligned}
&\sum_{n=0}^{\infty} -i\eta_n(y)\cos(\gamma\, nz)\alpha\, c + \sum_{n=0}^{\infty} i\eta_n(y)\cos(\gamma\, nz)\alpha\; U_0(y) \\
&+\sum_{n=0}^{\infty} 1/2\, i\eta_n(y)\alpha\, U_s(y)\cos(\gamma\, nz-\gamma\, z) + \sum_{n=0}^{\infty} 1/2\, i\eta_n(y)\alpha\, U_s(y)\cos(\gamma\, nz+\gamma\, z) \\
&+\sum_{n=0}^{\infty} \frac{\cos(\gamma\, nz)\eta_n(y)\alpha^2}{\mathrm{Re}} + \sum_{n=0}^{\infty} -\frac{\left(\frac{d^2}{dy^2}\eta_n(y)\right)\cos(\gamma\, nz)}{\mathrm{Re}} \\
&+\sum_{n=0}^{\infty} \frac{\eta_n(y)\cos(\gamma\, nz)\gamma^2 n^2}{\mathrm{Re}} + \sum_{n=1}^{\infty} 1/2\, U_s(y)\gamma\, \left(\frac{d}{dy}v_n(y)\right)\cos(\gamma\, z-\gamma\, nz) \\
&+\sum_{n=1}^{\infty} -1/2\, U_s(y)\gamma\, \left(\frac{d}{dy}v_n(y)\right)\cos(\gamma\, nz+\gamma\, z) + \sum_{n=1}^{\infty} v_n(y)\cos(\gamma\, nz)\gamma\, n\frac{d}{dy}U_0(y) \\
&+\sum_{n=1}^{\infty} 1/2\, v_n(y)\gamma\, n\left(\frac{d}{dy}U_s(y)\right)\cos(\gamma\, nz-\gamma\, z) + \sum_{n=1}^{\infty} 1/2\, v_n(y)\gamma\, n\left(\frac{d}{dy}U_s(y)\right)\cos(\gamma\, nz+\gamma\, z) \\
&+\sum_{n=1}^{\infty} -1/2\, \left(\frac{d}{dy}U_s(y)\right)\gamma\, v_n(y)\cos(\gamma\, z-\gamma\, nz) + \sum_{n=1}^{\infty} 1/2\, \left(\frac{d}{dy}U_s(y)\right)\gamma\, v_n(y)\cos(\gamma\, nz+\gamma\, z) \\
&+\sum_{n=0}^{\infty} -1/2\, U_s(y)\gamma^2 w_n(y)\cos(\gamma\, nz-\gamma\, z) + \sum_{n=0}^{\infty} -1/2\, U_s(y)\gamma^2 w_n(y)\cos(\gamma\, nz+\gamma\, z) \quad = \quad 0
\end{aligned}$$

C.2 Linearized mode-wise stability equations

Factoring trigonometric functions with identical argument in the relations of the above section C.1 and considering that the equalities require each coefficient to be zero independentely, one obtains the following relations, which differ according to the type of the fundamental solution considered and depend on the spanwise mode n.

C.2.1 Sinusoidal mode

normal velocity equation

$(n=1)$

$$\begin{aligned}
&2\,\left(\frac{d}{dy}U_s(y)\right)\gamma\, w_0(y) + 2\, U_s(y)\gamma\,\frac{d}{dy}w_0(y) - U_0(y)v_1(y)\gamma^2 + v_1(y)\gamma^2 c + \alpha^2 v_1(y)c \\
&-\alpha^2\, U_0(y)v_1(y) + U_0(y)\frac{d^2}{dy^2}v_1(y) + 2\,\frac{i\alpha\, v_1(y)\gamma^2}{\mathrm{Re}} \\
&-v_1(y)\frac{d^2}{dy^2}U_0(y) - 2\,\frac{i\alpha\,\frac{d^2}{dy^2}v_1(y)}{\mathrm{Re}} + \frac{i\alpha^3 v_1(y)}{\mathrm{Re}} - \left(\frac{d^2}{dy^2}v_1(y)\right)c \\
&-2\,\frac{i\left(\frac{d^2}{dy^2}v_1(y)\right)\gamma^2}{\alpha\,\mathrm{Re}} + \frac{i\frac{d^4}{dy^4}v_1(y)}{\alpha\,\mathrm{Re}} + \frac{iv_1(y)\gamma^4}{\alpha\,\mathrm{Re}} \\
&-\left(\frac{d}{dy}U_s(y)\right)\gamma\, w_2(y) + 1/2\, U_s(y)\frac{d^2}{dy^2}v_2(y) - 1/2\,\alpha^2 U_s(y)v_2(y) - 1/2\, U_s(y)v_2(y)\gamma^2 \qquad (59) \\
&-1/2\, v_2(y)\frac{d^2}{dy^2}U_s(y) - U_s(y)\gamma\,\frac{d}{dy}w_2(y) \quad = \quad 0
\end{aligned}$$

$(n \geq 2)$

$$
\begin{aligned}
U_s(y)v_{n-1}(y)(\gamma n)^2 + \frac{i\alpha^3 v_n(y)}{\mathrm{Re}} - 2\,\frac{i\alpha\,\frac{d^2}{dy^2}v_n(y)}{\mathrm{Re}} + \frac{i\frac{d^4}{dy^4}v_n(y)}{\alpha\,\mathrm{Re}} - \alpha^2\,U_0(y)v_n(y) \\
+\alpha^2 v_n(y)c + v_n(y)(\gamma n)^2 c - 1/2\,\alpha^2 U_s(y)v_{n-1}(y) - 1/2\,\alpha^2 U_s(y)v_{n+1}(y) \\
+\left(\frac{d}{dy}U_s(y)\right)\gamma\,w_{n-1}(y) + 2\,\frac{i\alpha\,v_n(y)(\gamma n)^2}{\mathrm{Re}} - U_s(y)\gamma\,\frac{d}{dy}w_{n+1}(y) - 2\,\frac{i\left(\frac{d^2}{dy^2}v_n(y)\right)(\gamma n)^2}{\alpha\,\mathrm{Re}} \\
-\frac{1}{2}U_s(y)v_{n+1}(y)(\gamma n)^2 - \left(\frac{d}{dy}U_s(y)\right)\gamma\,w_{n+1}(y) - U_0(y)v_n(y)(\gamma n)^2 \\
+U_s(y)\gamma\,\frac{d}{dy}w_{n-1}(y) + U_0(y)\frac{d^2}{dy^2}v_n(y) + 1/2\,U_s(y)\frac{d^2}{dy^2}v_{n+1}(y) \\
+1/2\,U_s(y)\frac{d^2}{dy^2}v_{n-1}(y) - v_n(y)\frac{d^2}{dy^2}U_0(y) - 1/2\,v_{n-1}(y)\frac{d^2}{dy^2}U_s(y) \\
-1/2\,v_{n+1}(y)\frac{d^2}{dy^2}U_s(y) - \left(\frac{d^2}{dy^2}v_n(y)\right)c + \frac{iv_n(y)(\gamma n)^4}{\alpha\,\mathrm{Re}} \quad = \quad 0
\end{aligned}
\tag{60}
$$

<u>normal vorticity equation</u>

$(n = 0)$

$$
\begin{aligned}
-\eta_0(y)c + \eta_0(y)\,U_0(y) - \frac{i\alpha\,\eta_0(y)}{\mathrm{Re}} + \frac{i\frac{d^2}{dy^2}\eta_0(y)}{\alpha\,\mathrm{Re}} + 1/2\,\eta_1(y)U_s(y) - 1/2\,\frac{iU_s(y)\gamma\,\frac{d}{dy}v_1(y)}{\alpha} \\
+1/2\,\frac{iU_s(y)\gamma^2 w_1(y)}{\alpha} \quad = \quad 0
\end{aligned}
\tag{61}
$$

$(n = 1)$

$$
\begin{aligned}
\eta_0(y)U_s(y) + \frac{iU_s(y)\gamma^2 w_0(y)}{\alpha} - \eta_1(y)c + \eta_1(y)\,U_0(y) - \frac{i\alpha\,\eta_1(y)}{\mathrm{Re}} + \frac{i\frac{d^2}{dy^2}\eta_1(y)}{\alpha\,\mathrm{Re}} \\
-\frac{i\eta_1(y)\gamma^2}{\alpha\,\mathrm{Re}} - \frac{iv_1(y)\gamma\,\frac{d}{dy}U_0(y)}{\alpha} + 1/2\,\eta_2(y)U_s(y) - 1/2\,\frac{iU_s(y)\gamma\,\frac{d}{dy}v_2(y)}{\alpha} \\
-1/2\,\frac{iv_2(y)\gamma\,\frac{d}{dy}U_s(y)}{\alpha} + 1/2\,\frac{iU_s(y)\gamma^2 w_2(y)}{\alpha} \quad = \quad 0
\end{aligned}
\tag{62}
$$

$(n \geq 2)$

$$
\begin{aligned}
1/2\,\eta_{n-1}(y)U_s(y) + 1/2\,\frac{iU_s(y)\gamma\,\frac{d}{dy}v_{n-1}(y)}{\alpha} - \frac{iv_{n-1}(y)\gamma n\,\frac{d}{dy}U_s(y)}{2\alpha} + 1/2\,\frac{iU_s(y)\gamma^2 w_{n-1}(y)}{\alpha} \\
-\eta_n(y)c + \eta_n(y)\,U_0(y) - \frac{i\alpha\,\eta_n(y)}{\mathrm{Re}} + \frac{i\frac{d^2}{dy^2}\eta_n(y)}{\mathrm{Re}\,\alpha} - \frac{i\eta_n(y)(\gamma n)^2}{\mathrm{Re}\,\alpha} \\
-\frac{iv_n(y)\gamma n\,\frac{d}{dy}U_0(y)}{\alpha} + 1/2\,\eta_{n+1}(y)U_s(y) - 1/2\,\frac{iU_s(y)\gamma\,\frac{d}{dy}v_{n+1}(y)}{\alpha} - \frac{iv_{n+1}(y)\gamma n\,\frac{d}{dy}U_s(y)}{2\alpha} \\
+1/2\,\frac{iU_s(y)\gamma^2 w_{n+1}(y)}{\alpha} \quad = \quad 0
\end{aligned}
\tag{63}
$$

<u>stream- and spanwise velocity</u>

$$
(n = 0) \quad w_0 = +\frac{i}{\alpha}\,\eta_0
$$

$$
(n \geq 1) \quad u_n = \frac{i\alpha\,\frac{d}{dy}v_n(y) + \eta_n(y)\gamma\,n}{\alpha^2 + \gamma^2 n^2} w_n = \frac{i\alpha\,\eta_n(y) + \left(\frac{d}{dy}v_n(y)\right)\gamma\,n}{\alpha^2 + \gamma^2 n^2}\,. \tag{64}
$$

C.2.2 Varicose mode

normal velocity equation

$(n = 0)$

$$\begin{aligned}
&\frac{i\frac{d^4}{dy^4}v_0(y)}{\alpha\,\mathrm{Re}} - 2\,\frac{i\alpha\,\frac{d^2}{dy^2}v_0(y)}{\mathrm{Re}} - \alpha^2\,U_0(y)v_0(y) + U_0(y)\frac{d^2}{dy^2}v_0(y) + \alpha^2 v_0(y)c + \frac{i\alpha^3 v_0(y)}{\mathrm{Re}} \\
&\quad - \left(\frac{d^2}{dy^2}v_0(y)\right)c - v_0(y)\frac{d^2}{dy^2}U_0(y) + U_s(y)\gamma\,\frac{d}{dy}w_1(y) - 1/2\,\alpha^2 U_s(y)v_1(y) \qquad (65)\\
&\quad + 1/2\,U_s(y)\frac{d^2}{dy^2}v_1(y) + \left(\frac{d}{dy}U_s(y)\right)\gamma\,w_1(y) - 1/2\,v_1(y)\frac{d^2}{dy^2}U_s(y) \;=\; 0
\end{aligned}$$

$(n = 1)$

$$\begin{aligned}
&-\alpha^2 U_s(y)v_0(y) + U_s(y)\frac{d^2}{dy^2}v_0(y) - v_0(y)U_s(y)\gamma^2 - v_0(y)\frac{d^2}{dy^2}U_s(y) - \alpha^2\,U_0(y)v_1(y) \\
&-U_0(y)v_1(y)\gamma^2 + \frac{i\frac{d^4}{dy^4}v_1(y)}{\alpha\,\mathrm{Re}} + \frac{i\alpha^3 v_1(y)}{\mathrm{Re}} + \frac{iv_1(y)\gamma^4}{\alpha\,\mathrm{Re}} - v_1(y)\frac{d^2}{dy^2}U_0(y) + 2\,\frac{i\alpha\,v_1(y)\gamma^2}{\mathrm{Re}} \\
&\quad + \alpha^2 v_1(y)c - \left(\frac{d^2}{dy^2}v_1(y)\right)c - 2\,\frac{i\left(\frac{d^2}{dy^2}v_1(y)\right)\gamma^2}{\alpha\,\mathrm{Re}} + v_1(y)\gamma^2 c - 2\,\frac{i\alpha\,\frac{d^2}{dy^2}v_1(y)}{\mathrm{Re}} \qquad (66)\\
&\quad + U_0(y)\frac{d^2}{dy^2}v_1(y) - 1/2\,U_s(y)v_2(y)\gamma^2 - 1/2\,\alpha^2 U_s(y)v_2(y) + 1/2\,U_s(y)\frac{d^2}{dy^2}v_2(y) \\
&\quad + \left(\frac{d}{dy}U_s(y)\right)\gamma\,w_2(y) - 1/2\,v_2(y)\frac{d^2}{dy^2}U_s(y) + U_s(y)\gamma\,\frac{d}{dy}w_2(y) \;=\; 0
\end{aligned}$$

$(n \geq 2)$

$$\begin{aligned}
&\frac{i\alpha^3 v_n(y)}{\mathrm{Re}} - U_0(y)v_n(y)(\gamma n)^2 - \frac{1}{2}U_s(y)v_{n-1}(y)(\gamma n)^2 - \left(\frac{d}{dy}U_s(y)\right)\gamma\,w_{n-1}(y) \\
&\quad + U_s(y)\gamma\,\frac{d}{dy}w_{n+1}(y) - 2\,\frac{i\alpha\,\frac{d^2}{dy^2}v_n(y)}{\mathrm{Re}} + \frac{i\frac{d^4}{dy^4}v_n(y)}{\mathrm{Re}\,\alpha} + \left(\frac{d}{dy}U_s(y)\right)\gamma\,w_{n+1}(y) \\
&+ v_n(y)(\gamma n)^2 c + \alpha^2 v_n(y)c - \alpha^2\,U_0(y)v_n(y) - 1/2\,\alpha^2 U_s(y)v_{n+1}(y) - \frac{1}{2}U_s(y)v_{n+1}(y)(\gamma n)^2 \\
&\quad - U_s(y)\gamma\,\frac{d}{dy}w_{n-1}(y) + 2\,\frac{i\alpha\,v_n(y)(\gamma n)^2}{\mathrm{Re}} \\
&- \frac{i\left(\frac{d^2}{dy^2}v_n(y)\right)(\gamma n)^2}{\mathrm{Re}\,\alpha} + \frac{iv_n(y)(\gamma n)^4}{\mathrm{Re}\,\alpha} + 1/2\,U_s(y)\frac{d^2}{dy^2}v_{n+1}(y) + 1/2\,U_s(y)\frac{d^2}{dy^2}v_{n-1}(y) \qquad (67)\\
&\quad - 1/2\,v_{n-1}(y)\frac{d^2}{dy^2}U_s(y) - 1/2\,v_{n+1}(y)\frac{d^2}{dy^2}U_s(y) - v_n(y)\frac{d^2}{dy^2}U_0(y) - \left(\frac{d^2}{dy^2}v_n(y)\right)c \\
&\quad + U_0(y)\frac{d^2}{dy^2}v_n(y) - 1/2\,\alpha^2 U_s(y)v_{n-1}(y) \;=\; 0
\end{aligned}$$

normal vorticity equation

$(n = 1)$

$$-\frac{iU_s(y)\gamma\,\frac{d}{dy}v_0(y)}{\alpha} + \frac{i\left(\frac{d}{dy}U_s(y)\right)\gamma\,v_0(y)}{\alpha} - \eta_1(y)c + \eta_1(y)\,U_0(y) - \frac{i\alpha\,\eta_1(y)}{\mathrm{Re}}$$

$$+\frac{i\frac{d^2}{dy^2}\eta_1(y)}{\alpha\,\mathrm{Re}}-\frac{i\eta_1(y)\gamma^2}{\alpha\,\mathrm{Re}}+\frac{iv_1(y)\gamma\,\frac{d}{dy}U_0(y)}{\alpha}+1/2\,\eta_2(y)U_s(y)+1/2\,\frac{iU_s(y)\gamma\,\frac{d}{dy}v_2(y)}{\alpha} \tag{68}$$
$$+1/2\,\frac{iv_2(y)\gamma\,\frac{d}{dy}U_s(y)}{\alpha}+1/2\,\frac{iU_s(y)\gamma^2w_2(y)}{\alpha} \quad = \quad 0$$

$(n \geq 2)$

$$1/2\,\eta_{n-1}(y)U_s(y)-1/2\,\frac{iU_s(y)\gamma\,\frac{d}{dy}v_{n-1}(y)}{\alpha}+\frac{iv_{n-1}(y)\gamma n\,\frac{d}{dy}U_s(y)}{2\alpha}+1/2\,\frac{iU_s(y)\gamma^2w_{n-1}(y)}{\alpha}$$
$$-\eta_n(y)c+\eta_n(y)\,U_0(y)-\frac{i\alpha\,\eta_n(y)}{\mathrm{Re}}+\frac{i\frac{d^2}{dy^2}\eta_n(y)}{\alpha\,\mathrm{Re}}-\frac{i\eta_n(y)(\gamma n)^2}{\alpha\,\mathrm{Re}}$$
$$+\frac{iv_n(y)\gamma n\,\frac{d}{dy}U_0(y)}{2\alpha}+1/2\,\eta_{n+1}(y)U_s(y)+1/2\,\frac{iU_s(y)\gamma\,\frac{d}{dy}v_{n+1}(y)}{\alpha} \tag{69}$$
$$+\frac{iv_{n+1}(y)\gamma n\,\frac{d}{dy}U_s(y)}{2\alpha}+1/2\,\frac{iU_s(y)\gamma^2w_{n+1}(y)}{\alpha} \quad = \quad 0$$

stream- and spanwise velocity

$$(n=0) \quad u_0=-\frac{1}{i\,\alpha}\,\frac{d}{dy}v_0$$

$$(n\geq 1) \quad u_n=-\frac{-i\,\alpha\,\frac{d}{dy}v_n(y)+\eta_n(y)\gamma\,n}{\alpha^2+\gamma^2n^2}\,, \qquad w_n=-\frac{-i\,\alpha\,\eta_n(y)+\left(\frac{d}{dy}v_n(y)\right)\gamma\,n}{\alpha^2+\gamma^2n^2}\,. \tag{70}$$

C.2.3 Subharmonic mode

normal velocity equation

$(n=0)$

$$1/2\,\frac{i\alpha\,v_0(y)\gamma^2}{rey}+1/16\,\frac{iv_0(y)\gamma^4}{\alpha\,rey}-1/2\,\frac{i\left(\frac{d^2}{dy^2}v_0(y)\right)\gamma^2}{\alpha\,rey}+\frac{i\alpha^3v_0(y)}{rey}$$
$$+\frac{i\frac{d^4}{dy^4}v_0(y)}{\alpha\,rey}-2\,\frac{i\alpha\,\frac{d^2}{dy^2}v_0(y)}{rey}-1/2\,v_1(y)\frac{d^2}{dy^2}U_s(y)+1/2\,U_s(y)\frac{d^2}{dy^2}v_1(y) \tag{71}$$
$$+U_0(y)\frac{d^2}{dy^2}v_0(y)-1/2\,U_s(y)\frac{d^2}{dy^2}v_0(y)+1/2\,v_0(y)\frac{d^2}{dy^2}U(y)-\left(\frac{d^2}{dy^2}v_0(y)\right)c-\alpha^2U_0(y)v_0(y)$$
$$+\alpha^2v_0(y)c+U_s(y)\gamma\,\frac{d}{dy}w_0(y)+1/8\,U_s(y)\gamma^2v_0(y)+1/4\,v_0(y)\gamma^2c-1/2\,\alpha^2U_s(y)v_1(y)$$
$$-\left(\frac{d}{dy}U_s(y)\right)\gamma\,w_1(y)-1/8\,U_s(y)\gamma^2v_1(y)-U_s(y)\gamma\,\frac{d}{dy}w_1(y)-1/4\,U_0(y)v_0(y)\gamma^2$$
$$+\left(\frac{d}{dy}U_s(y)\right)\gamma\,w_0(y)-v_0(y)\frac{d^2}{dy^2}U_0(y)+1/2\,\alpha^2U_s(y)v_0(y) \quad = \quad 0$$

$(n\geq 1)$

$$-v_n(y)\frac{d^2}{dy^2}\,U_0(y)-1/2\,v_{n+1}(y)\frac{d^2}{dy^2}U_s(y)+1/2\,U_s(y)\frac{d^2}{dy^2}v_{n+1}(y)+\,U_0(y)\frac{d^2}{dy^2}v_n(y)$$
$$-\left(\frac{d^2}{dy^2}v_n(y)\right)c-1/2\,\alpha^2U_s(y)v_{n-1}(y)+\left(\frac{d}{dy}U_s(y)\right)\gamma\,w_{n-1}(y)$$

$$
\begin{aligned}
&-\frac{1}{8}\,U_s(y)(\frac{(2n+1)}{2}\gamma)^2\,v_{n-1}(y)+U_s(y)\gamma\,\frac{d}{dy}w_{n-1}(y)-1/2\,v_{n-1}(y)\frac{d^2}{dy^2}U_s(y)+1/2\,U_s(y)\frac{d^2}{dy^2}v_{n-1}(y) \qquad (72)\\
&-U_s(y)\gamma\,\frac{d}{dy}w_{n+1}(y)-\left(\frac{d}{dy}U_s(y)\right)\gamma\,w_{n+1}(y)-1/2\,\alpha^2U_s(y)v_{n+1}(y)-\frac{1}{2}\,U_s(y)(\frac{(2n+1)}{2}\gamma)^2\,v_{n+1}(y)\\
&-U_0(y)v_n(y)(\frac{(2n+1)}{2}\gamma)^2+v_n(y)(\frac{(2n+1)}{2}\gamma)^2\,c-\alpha^2\,U_0(y)v_n(y)+\alpha^2v_n(y)c\\
&-2\,\frac{i\alpha\,\frac{d^2}{dy^2}v_n(y)}{rey}+\frac{i\alpha^3v_n(y)}{rey}+\frac{i\frac{d^4}{dy^4}v_n(y)}{\alpha\,rey}+2\,\frac{i\alpha\,v_n(y)(\frac{(2n+1)}{2}\gamma)^2}{rey}\\
&+\frac{iv_n(y)(\frac{(2n+1)}{2}\gamma)^4}{\alpha\,rey}-2\,\frac{i\left(\frac{d^2}{dy^2}v_n(y)\right)(\frac{(2n+1)}{2}\gamma)^2}{\alpha\,rey} \;=\; 0
\end{aligned}
$$

normal vorticity equation

$(n=0)$

$$
\begin{aligned}
&1/2\,\eta_0(y)U_s(y)+\frac{i\frac{d^2}{dy^2}\eta_0(y)}{\alpha\,rey}-1/2\,\frac{iU_s(y)\gamma\,\frac{d}{dy}v_0(y)}{\alpha}-1/2\,\frac{iv_0(y)\gamma\,\frac{d}{dy}U_0(y)}{\alpha}\\
&+1/4\,\frac{i\left(\frac{d}{dy}U_s(y)\right)\gamma\,v_0(y)}{\alpha}+1/2\,\frac{iU_s(y)\gamma^2w_0(y)}{\alpha}+\eta_0(y)\,U_0(y)-1/4\,\frac{i\eta_0(y)\gamma^2}{\alpha\,rey}-\frac{i\alpha\,\eta_0(y)}{rey} \qquad (73)\\
&-\eta_0(y)c+1/2\,\eta_1(y)U_s(y)-1/2\,\frac{iU_s(y)\gamma\,\frac{d}{dy}v_1(y)}{\alpha}-1/4\,\frac{iv_1(y)\gamma\,\frac{d}{dy}U_s(y)}{\alpha}+1/2\,\frac{iU_s(y)\gamma^2w_1(y)}{\alpha} \;=\; 0
\end{aligned}
$$

$(n\geq 1)$

$$
\begin{aligned}
&1/2\,\eta_{n-1}(y)U_s(y)+1/2\,\frac{iU_s(y)\gamma\,\frac{d}{dy}v_{n-1}(y)}{\alpha}-\frac{(2n+1)}{4}\,\frac{i\left(\frac{d}{dy}U_s(y)\right)\gamma\,v_{n-1}(y)}{\alpha}\\
&+1/2\,\frac{iU_s(y)\gamma^2w_{n-1}(y)}{\alpha}-\frac{i\alpha\,\eta_n(y)}{rey}+\frac{i\frac{d^2}{dy^2}\eta_n(y)}{rey\,\alpha}\\
&-\frac{i\eta_n(y)(\frac{(2n+1)}{2}\gamma)^2}{rey\,\alpha}-\frac{(2n+1)}{2}\,\frac{iv_n(y)\gamma\,\frac{d}{dy}U_0(y)}{\alpha}+\eta_n(y)\,U_0(y)-\eta_n(y)c+1/2\,\eta_{n+1}(y)U_s(y) \qquad (74)\\
&-1/2\,\frac{iU_s(y)\gamma\,\frac{d}{dy}v_{n+1}(y)}{\alpha}-\frac{(2n+1)}{4}\,\frac{iv_{n+1}(y)\gamma\,\frac{d}{dy}U_s(y)}{\alpha}+1/2\,\frac{iU_s(y)\gamma^2w_{n+1}(y)}{\alpha} \;=\; 0
\end{aligned}
$$

stream- and spanwise velocity

$$
\begin{aligned}
(n\geq 0)\qquad u_n &= 2\,\frac{i\left(2\,\left(\frac{d}{dy}v_n(y)\right)\alpha-2\,i\gamma\,n\eta_n(y)-i\gamma\,\eta_n(y)\right)}{4\,\alpha^2+4\,\gamma^2n^2+4\,\gamma^2n+\gamma^2}\,,\\
w_n &= -2\,\frac{i\left(2\,i\gamma\,n\frac{d}{dy}v_n(y)+i\gamma\,\frac{d}{dy}v_n(y)-2\,\eta_n(y)\alpha\right)}{4\,\alpha^2+4\,\gamma^2n^2+4\,\gamma^2n+\gamma^2}\,. \qquad (75)
\end{aligned}
$$

In the above expressions, we note – besides the obvious coupling of all four equations – the coupling of any spanwise mode n with its immediate neighbours $n-1$ and $n+1$ which is a consequence of the spanwise cosine variation of the streak amplitude.

C.3 The discretization of the streak instability problem

The discretization of equations (59)–(75) pertinent to the streak instability problem, using a Galerkin MWR apporach, leads to relations of the following type, respectively for v and η:

$$\begin{aligned} [a_{n-1}]\cdot\hat{v}_{n-1} + [a_n]\cdot\hat{v}_n + [a_{n+1}]\cdot\hat{v}_{n+1} & \\ + [b_{n-1}]\cdot\hat{\eta}_{n-1} + [b_{n+1}]\cdot\hat{\eta}_{n+1} &= c\cdot[d_n]\cdot\hat{v}_n\,, \end{aligned} \tag{76}$$

$$\begin{aligned} [e_{n-1}]\cdot\hat{v}_{n-1} + [e_n]\cdot\hat{v}_n + [e_{n+1}]\cdot\hat{v}_{n+1} & \\ + [f_{n-1}]\cdot\hat{\eta}_{n-1} + [f_n]\cdot\hat{\eta}_n + [f_{n+1}]\cdot\hat{\eta}_{n+1} &= c\cdot[g_n]\cdot\hat{\eta}_n\,, \end{aligned} \tag{77}$$

where the coefficients a_i, b_i, d_i, e_i, f_i, g_i are functions of the matrices M_{40}, $\widetilde{M}(\hat{U}_0)$, $\widetilde{M}(\hat{U}_s)$, $\widetilde{K}(\hat{U}_0)$, $\widetilde{K}(\hat{U}_s)$, $\widetilde{\widetilde{M}}(\hat{U}_0)$, $\widetilde{\widetilde{M}}(\hat{U}_s)$, K and M defined in (56) as well as the supplementary matrices consisting of triple integrals of b-spline functions $D(\hat{U}_0)$, $D(\hat{U}_s)$, $\widetilde{D}(\hat{U}_0)$, $\widetilde{D}(\hat{U}_s)$, $S(\hat{U}_0)$, $S(\hat{U}_s)$ defined as follows:

$$\begin{aligned} \widetilde{D}_{ij}(\hat{U}) &= \sum_k \hat{U}_k \int_0^{L_y} B_k'(y)\, B_j(y)\, B_i(y)\,\mathrm{d}y \\ \widetilde{D}_{ij}(\hat{U}) &= \sum_k \hat{U}_k \int_0^{L_y} B_k(y)\, B_j'(y)\, B_i(y)\,\mathrm{d}y \\ S_{ij}(\hat{U}) &= \sum_k \hat{U}_k \int_0^{L_y} B_k'(y)\, B_j'(y)\, B_i(y)\,\mathrm{d}y\,. \end{aligned} \tag{78}$$

The above cited 9 different types of matrices (where additionally in 6 cases the argument can be either the coefficients of the turbulent base profile $\hat{U}_0$ or of the streak contribution $\hat{U}_s$) can again be precalculated for a given b-spline base. The task consists then of assembling the matrices A and B of the general system $A\cdot\hat{x} = c\cdot B\cdot\hat{x}$ for a given number of modes N_z according to the discrete equations (76) and (77). The matrix structure of this system is symbolically depicted in figure 15. The coupling between the equations for v and η is reflected by the entries in the quadrants I and III of matrix A, wheras the spanwise mode coupling gives rise to the overall block-tridiagonal structure.

C.4 Numerical treatment of boundary conditions

Again using a b-spline collocation method, the boundary conditions for the velocity and vorticity equation take the following form:

$$\begin{aligned} \sum_j \hat{\eta}_n^j\, B_j(y = y_w) &= 0 \qquad\qquad y_w = \{0, 2\} \\ \sum_j \hat{v}_n^j\, B_j'(y = y_w) &= 0 \\ \sum_j \hat{v}_n^j\, B_j(y = 2) &= 0 \quad , \end{aligned} \tag{79}$$

where the subscript of the coefficient indicates the spanwise mode and the superscript the b-spline coefficient index. The missing condition for v on the lower wall is simply

$$\sum_j \hat{v}_n^j\, B_j(y = 0) \;=\; 0 \quad , \tag{80}$$

for an impermeable wall. In the general case of a porous wall ($\beta \neq 0$), the latter condition becomes one of the following:

sinusoidal mode

$(n=1)$

$$\beta\left[\sum_k \hat{U}_0^k\, B_k'(y=0)\sum_j \hat{v}_1^j\, B_j(y=0)+\frac{1}{2}\sum_k \hat{U}_s^k\, B_k'(y=0)\sum_j \hat{v}_2^j\, B_j(y=0)\right.$$
$$\left.-\frac{1}{\mathrm{Re}}u_1''(y=0)\right]-i\alpha\sum_j \hat{v}_1^j\, B_j(y=0) \quad = \quad 0 \quad .$$

$(n\geq 2)$

$$\beta\left[\sum_k \hat{U}_0^k\, B_k'(y=0)\sum_j \hat{v}_n^j\, B_j(y=0)+\frac{1}{2}\sum_k \hat{U}_s^k\, B_k'(y=0)\sum_j \hat{v}_{n-1}^j\, B_j(y=0)\right.$$
$$\left.+\frac{1}{2}\sum_k \hat{U}_s^k\, B_k'(y=0)\sum_j \hat{v}_{n+1}^j\, B_j(y=0)-\frac{1}{\mathrm{Re}}\,u_n''(y=0)\right]-i\alpha\sum_j \hat{v}_n^j\, B_j(y=0) \quad = \quad 0 \quad .$$

varicose mode

$(n=0)$

$$\beta\left[\sum_k \hat{U}_0^k\, B_k'(y=0)\sum_j \hat{v}_0^j\, B_j(y=0)+\frac{1}{2}\sum_k \hat{U}_s^k\, B_k'(y=0)\sum_j \hat{v}_1^j\, B_j(y=0)\right.$$
$$\left.-\frac{1}{\mathrm{Re}}\,u_0''(y=0)\right]-i\alpha\sum_j \hat{v}_0^j\, B_j(y=0) \quad = \quad 0 \quad .$$

$(n=1)$

$$\beta\left[\sum_k \hat{U}_0^k\, B_k'(y=0)\sum_j \hat{v}_1^j\, B_j(y=0)+\sum_k \hat{U}_s^k\, B_k'(y=0)\sum_j \hat{v}_0^j\, B_j(y=0)\right.$$
$$\left.+\frac{1}{2}\sum_k \hat{U}_s^k\, B_k'(y=0)\sum_j \hat{v}_2^j\, B_j(y=0)-\frac{1}{\mathrm{Re}}\,u_1''(y=0)\right]-i\alpha\sum_j \hat{v}_1^j\, B_j(y=0) \quad = \quad 0 \quad .$$

$(n\geq 2)$

$$\beta\left[\sum_k \hat{U}_0^k\, B_k'(y=0)\sum_j \hat{v}_n^j\, B_j(y=0)+\frac{1}{2}\sum_k \hat{U}_s^k\, B_k'(y=0)\sum_j \hat{v}_{n-1}^j\, B_j(y=0)\right.$$
$$\left.+\frac{1}{2}\sum_k \hat{U}_s^k\, B_k'(y=0)\sum_j \hat{v}_{n+1}^j\, B_j(y=0)-\frac{1}{\mathrm{Re}}\,u_n''(y=0)\right]-i\alpha\sum_j \hat{v}_n^j\, B_j(y=0) \quad = \quad 0 \quad .$$

subharmonic mode

$(n=0)$

$$\beta\left[\sum_k \hat{U}_0^k\, B_k'(y=0)\sum_j \hat{v}_0^j\, B_j(y=0)-\frac{1}{2}\sum_k \hat{U}_s^k\, B_k'(y=0)\sum_j \hat{v}_0^j\, B_j(y=0)\right.$$
$$\left.+\frac{1}{2}\sum_k \hat{U}_s^k\, B_k'(y=0)\sum_j \hat{v}_1^j\, B_j(y=0)-\frac{1}{\mathrm{Re}}\,u_0''(y=0)\right]-i\alpha\sum_j \hat{v}_0^j\, B_j(y=0) \quad = \quad 0 \quad .$$

$(n \geq 1)$

$$\beta \left[\sum_k \hat{U}_0^k \, B_k'(y=0) \sum_j \hat{v}_n^j \, B_j(y=0) + \frac{1}{2} \sum_k \hat{U}_s^k \, B_k'(y=0) \sum_j \hat{v}_{n-1}^j \, B_j(y=0) \right.$$

$$\left. + \frac{1}{2} \sum_k \hat{U}_s^k \, B_k'(y=0) \sum_j \hat{v}_{n+1}^j \, B_j(y=0) - \frac{1}{\mathrm{Re}} \, u_n''(y=0) \right] - i\alpha \sum_j \hat{v}_n^j \, B_j(y=0) \quad = \quad 0 \quad .$$

In our Galerkin-tau approach, the above relations are introduced directly into matrices A and B of the discretized system, i.e. in each "stripe" of length N_s four lines are replaced in the upper half of the system and two lines in the lower half. Performing the Gauss elimination technique suggested by Mizushima (see section B.5) was found to be rather cumbersome in this context. We opted for a direct computation of the eigenvalues of the full system which evidently leads to a number of zero-valued left eigenvalues coresponding to the number of zero-valued lines in matrix B (roughly a number of $(4+2)N_z$). We can thus distinguish and discard these eigenvalues.

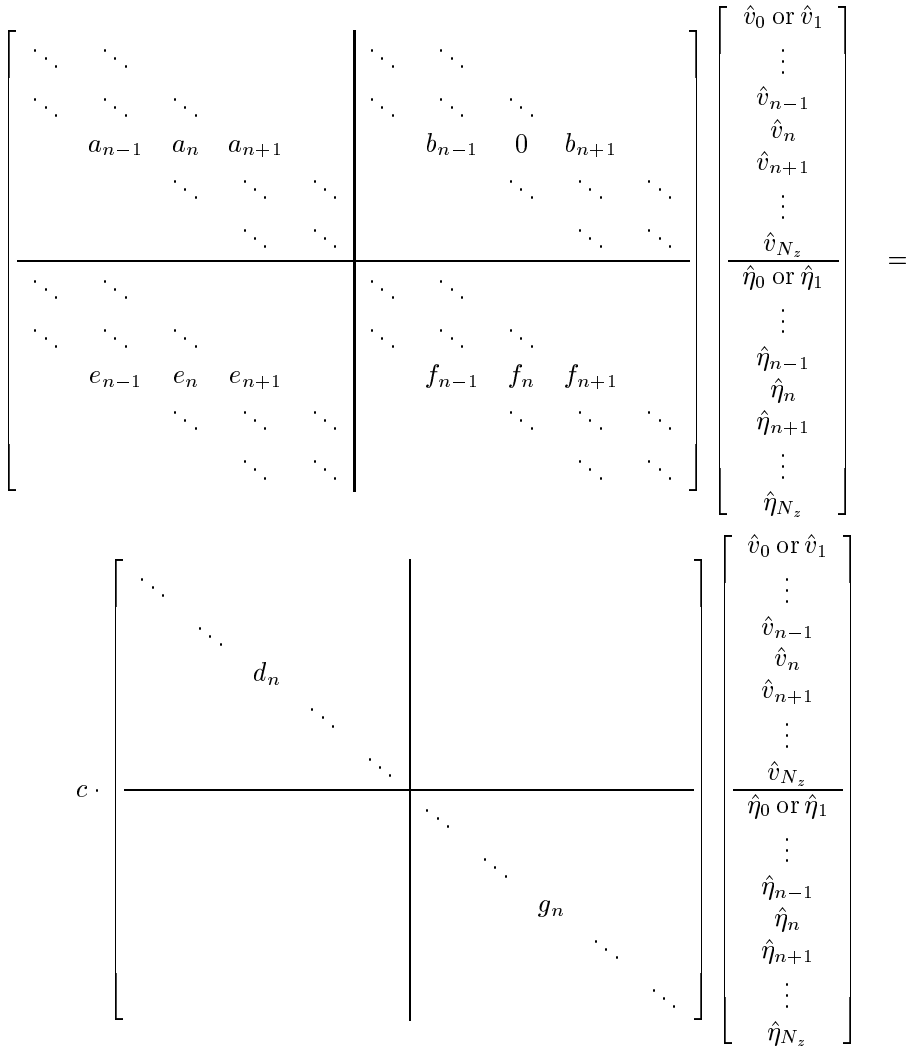

Figure 15: Structure of the general system of algebraic equations arising from the discretization of the stability problem of streak model flow. The entries a_i, b_i, d_i, e_i, f_i, g_i represent blocks of size $N_s \cdot N_s$ (being $(2k-1)$-diagonal), where N_s is the number of b-splines used in wall-normal direction. The quadrants of the two matrices have varying sizes according to the type of fundamental solution considered: from $N_z \cdot N_z$ to $(N_z+1) \cdot (N_z+1)$ blocks.

D MAPLE sources for the stability problem

D.1 Derivation of the streak instability equations, modewise

```
restart:
#-------------------------------------------------------------
print(‘STABILITY OF STREAKY FLOW‘);
print(‘----------------------------‘);
print(‘deriving the mode-coupled equations from the basic set of differential
         equations according to the type of fundamental solution‘);
print(‘‘);
print(‘DATE: 07.08.1998‘);
print(‘====================================‘);
print(‘NOTE: set the variable "mode" to {1,2,3} for {varicose,sinus,subharm}‘);
print();
#-------------------------------------------------------------
print(‘definition of laplacian of v-velocity:‘);
phi(x,y,z,t):=diff(v(x,y,z,t),x,x)+diff(v(x,y,z,t),y,y)+diff(v(x,y,z,t),z,z);
U(y,z):=U0(y)+U(y)*cos(gamma*z);
print(‘basic equation for v-velocity (EQUV=0)‘);
equv:=diff(phi(x,y,z,t),t)+U(y,z)*diff(phi(x,y,z,t),x)-(diff(phi(x,y,z,t),y,y)+
diff(phi(x,y,z,t),z,z)+diff(phi(x,y,z,t),x,x))/rey-(diff(U(y,z),y,y)-
diff(U(y,z),z,z))*diff(v(x,y,z,t),x)-2*diff(U(y,z),z)*(diff(w(x,y,z,t),x,y)-
diff(v(x,y,z,t),x,z))-2*diff(U(y,z),y,z)*diff(w(x,y,z,t),x);
print(‘basic y-vorticity equatio:‘);
equom:=diff(eta(x,y,z,t),t)+U(y,z)*diff(eta(x,y,z,t),x)-(diff(eta(x,y,z,t),x,x)+
diff(eta(x,y,z,t),y,y)+diff(eta(x,y,z,t),z,z))/rey-diff(U(y,z),z)*
diff(v(x,y,z,t),y)+diff(U(y,z),y)*diff(v(x,y,z,t),z)+
diff(U(y,z),y,z)*v(x,y,z,t)+diff(U(y,z),z,z)*w(x,y,z,t);
print(‘continuity equation:‘);
equcont:=diff(u(x,y,z,t),x)+diff(v(x,y,z,t),y)+diff(w(x,y,z,t),z);
print(‘definition of vorticity:‘);
defeta:=diff(u(x,y,z,t),z)-diff(w(x,y,z,t),x);
#
print(‘‘);
print(‘normal mode solution:‘);
u(x,y,z,t):=ut(y,z)*exp(I*alpha*(x-c*t));
v(x,y,z,t):=vt(y,z)*exp(I*alpha*(x-c*t));
w(x,y,z,t):=wt(y,z)*exp(I*alpha*(x-c*t));
eta(x,y,z,t):=etat(y,z)*exp(I*alpha*(x-c*t));
# 1- varicose, 2-sinusoidal, 3-subharmonic
mode:=1:
if (mode=1)then
#---varicose mode------
print(‘---VARICOSE MODE ----‘);
print(‘attention: the sums will be inserted later...‘);
#ut(y,z):=sum(u[n](y)*cos(gamma*n*z),n=0..infinity);
#ut(y,z):=sum(un(y)*cos(gamma*n*z),n=n0..ninf);
#vt(y,z):=sum(vn(y)*cos(gamma*n*z),n=n0..ninf);
#wt(y,z):=sum(wn(y)*sin(gamma*n*z),n=n1..ninf);
#etat(y,z):=sum(etan(y)*sin(gamma*n*z),n=n1..ninf);
ut(y,z):=un(y)*cos(gamma*n*z);
vt(y,z):=vn(y)*cos(gamma*n*z);
```

```
wt(y,z):=sum_from_one*wn(y)*sin(gamma*n*z);
etat(y,z):=sum_from_one*etan(y)*sin(gamma*n*z);
#
elif (mode=2)then
#---sinusoidal mode------
print(‘---SINUSOIDAL MODE ----‘);
print(‘attention: the sums will be inserted later...‘);
ut(y,z):=sum_from_one*un(y)*sin(gamma*n*z);
vt(y,z):=sum_from_one*vn(y)*sin(gamma*n*z);
wt(y,z):=wn(y)*cos(gamma*n*z);
etat(y,z):=etan(y)*cos(gamma*n*z);
#
elif (mode=3)then
#---subharmonic mode------
print(‘attention: the sums will be inserted later...‘);
print(‘---SUBHARMONIC MODE ----‘);
ut(y,z):=un(y)*sin(gamma*(n+1/2)*z);
vt(y,z):=vn(y)*sin(gamma*(n+1/2)*z);
wt(y,z):=wn(y)*cos(gamma*(n+1/2)*z);
etat(y,z):=etan(y)*cos(gamma*(n+1/2)*z);
fi;
#--------------PROCEDURE TO FIND STRING IN EXPRESSION: subs sum over nup-----
find_string:=proc(expr1,string1,nup) local expr2,flag,i,j,k,nopse,
nopsee,temp,temp2:
nopse:=nops(expr1):
temp:=0:temp2:=0:
expr2:=array(1..100):
for i from 1 to nopse do
  nopsee:=nops(op(i,expr1)):
  flag:=0:
  for j from 1 to nopsee do
    if(type(op(j,op(i,expr1)),string))then
      if(op(j,op(i,expr1))=string1)then
# print(‘operand‘,i,‘suboperand‘,j);
flag:=1;
      fi;
    fi;
  od;
  temp:=op(i,expr1);
  if(flag=1)then
    expr2[i]:=sum(temp/string1,n=1..nup):
  else
    expr2[i]:=sum(temp,n=0..nup):
  fi:
od;
sum(expr2[k],k=1..nopse);
end:
#-----------------------------------------------------
#--------------PROCEDURE TO FIND STRING IN EXPRESSION:subs nup---------
find_string2:=proc(expr1,string1,nup) local expr2,flag,i,j,k,nopse,nopsee,
temp,temp2:
nopse:=nops(expr1):
temp:=0:temp2:=0:
expr2:=array(1..100):
```

```
for i from 1 to nopse do
  nopsee:=nops(op(i,expr1)):
  flag:=0:
  for j from 1 to nopsee do
    if(type(op(j,op(i,expr1)),string))then
      if(op(j,op(i,expr1))=string1)then
# print(‘operand‘,i,‘suboperand‘,j);
flag:=1;
      fi;
    fi;
  od;
  temp:=op(i,expr1);
  if(flag=1)then
if(nup <> 0)then
          expr2[i]:=eval(subs({n=nup,vn(y)=v[nup](y),un(y)=u[nup](y),
                    wn(y)=w[nup](y),
                    etan(y)=eta[nup](y)},temp/string1)):
else
          expr2[i]:=0:
#          print(‘left out:‘,nup,i,j);
        fi:
  else
    expr2[i]:=eval(subs({n=nup,vn(y)=v[nup](y),un(y)=u[nup](y),wn(y)=w[nup](y),
etan(y)=eta[nup](y)},temp)):
  fi:
od;
sum(expr2[k],k=1..nopse);
end:
#-------------------------------------------------
#-----------------PROCEDURE TO COMBINE EXPRESSIONS--------------------
com_exp:=proc(expr1) local i,j,expr2,nopse;
nopse:=nops(expr1):
expr2:=array(1..100):
for i from 1 to nopse do
expr2[i]:=combine(op(i,expr1)):
od:
sum(expr2[j],j=1..nopse);
end:
#-------------------------------------------------------------------------
print(‘working on: v-velocity equation...‘);
equv:=simplify(eval(equv/exp(I*alpha*(x-c*t)))):
print(‘working on: y-vorticity equation...‘);
equom:=simplify(eval(equom/exp(I*alpha*(x-c*t)))):
print(‘working on continuity equation...‘);
equcont:=simplify(eval(equcont/exp(I*alpha*(x-c*t)))):
#defeta=sum(eta[n](y)*sin(gamma*n*z),n=1..infinity);
defeta:=simplify(eval(defeta/exp(I*alpha*(x-c*t)))):
#---combine the trigonometric expressions----------
print(‘v-velocity equation: combining trig. expressions...‘);
equv2:=com_exp(expand(equv)):
print(‘y-vorticity equation: combining trig. expressions...‘);
equom2:=com_exp(expand(equom)):
#---insert the sums according to keyword----------
print(‘=========================================================‘);
```

```
print(‘now, we insert the sums over spanwise wavenumber...‘);
print(‘(this can take a few minutes)‘);
equv3:=find_string(equv2,’sum_from_one’,infinity):
equom3:=find_string(equom2,’sum_from_one’,infinity):
print(‘--> general equations with series:‘);
print(‘V:____   ZERO=‘,equv3);
print(‘ETA:___   ZERO=‘,equom3);
#----write for a given finite upper wavenumber and collect-----
print(‘now, we calculate the expressions for n={0,1,2,3,4}...‘);
equv_0:=find_string2(equv2,’sum_from_one’,0):
equom_0:=find_string2(equom2,’sum_from_one’,0):
equv_1:=find_string2(equv2,’sum_from_one’,1):
equom_1:=find_string2(equom2,’sum_from_one’,1):
equv_2:=find_string2(equv2,’sum_from_one’,2):
equom_2:=find_string2(equom2,’sum_from_one’,2):
equv_3:=find_string2(equv2,’sum_from_one’,3):
equom_3:=find_string2(equom2,’sum_from_one’,3):
equv_4:=find_string2(equv2,’sum_from_one’,4):
equom_4:=find_string2(equom2,’sum_from_one’,4):
#-------PROCEDURE TO FIND MATCHING SINs & COSs---------
find_trig:=proc(expr1,nup,mode) local expr3,expr2,flag,i,j,k,l,ll,m,
mm,nopse,nopsee,temp,temp2,zero,flags,flagc,sub:
if(mode=3)then
  sub:=1/2:
else
  sub:=0:
fi:
nopse:=nops(expr1):
temp:=0:temp2:=0:
zero:=array(1..100):
expr2:=array(1..100,1..10):
expr3:=array(1..100,1..10):
#for each term i of the equation
for i from 1 to nopse do
  nopsee:=nops(op(i,expr1)):
  flags:=0:
  flagc:=0:
  #for each mode k
  for k from 1 to nup do
    #initialise
    expr2[i,k]:=0:expr3[i,k]:=0:
    #for each element j of term i of the equation
    for j from 1 to nopsee do
      if(op(j,op(i,expr1))=sin((k-sub)*gamma*z))then
expr2[i,k]:=op(i,expr1):
flags:=1:
      fi;
      if(op(j,op(i,expr1))=cos((k-sub)*gamma*z))then
expr3[i,k]:=op(i,expr1):
flagc:=1:
      fi;
    od:
  od:
  #if neither cos nor sin in the current term i then --> mode 0 term
```

```
  if(flags=0 and flagc=0)then
    zero[i]:=op(i,expr1):
  else
    zero[i]:=0:
  fi:
od:
[sum(zero[l],l=1..nopse)],[seq(sum(expr2[l,m],l=1..nopse),m=1..nup)],
[seq(sum(expr3[ll,mm],ll=1..nopse),mm=1..nup)];
end:
#-------------------------------------------------------
# flag for subharmonic mode
if(mode=3)then
  sub:=1/2:
else
  sub:=0:
fi:
#--------------------
print(`...and collect the terms with matching factors of sin & cos:`);
if(mode=3)then
  test[0]:=find_trig(expand(equv_0),6,mode):
  test[1]:=find_trig(expand(equv_1),6,mode):
  test[2]:=find_trig(expand(equv_2),6,mode):
  test[3]:=find_trig(expand(equv_3),6,mode):
  test[4]:=find_trig(expand(equv_4),6,mode):
else
  test[0]:=find_trig(equv_0,6,mode):
  test[1]:=find_trig(equv_1,6,mode):
  test[2]:=find_trig(equv_2,6,mode):
  test[3]:=find_trig(equv_3,6,mode):
  test[4]:=find_trig(equv_4,6,mode):
fi:
#
print(`----------------------I-----------------------------------------`);
print(`N=0, v-equation:`);
print(`------------------`);
ZERO:=expand((op(1,op(1,[test[0]]))+op(1,op(1,[test[1]]))+op(1,op(
1,[test[2]]))+op(1,op(1,[test[3]]))+op(1,op(1,[test[4]])))/(I*alpha));
#perhaps some collect or so ...
#
print(`N=1, v-equation:`);
print(`------------------`);
print(`(a) sin coefficients`);
ZERO:=expand((op(1,op(2,[test[0]]))+op(1,op(2,[test[1]]))+op(1,op(2,[test[2]]))+
op(1,op(2,[test[3]]))+op(1,op(2,[test[4]])))/(I*alpha*sin((1-sub)*gamma*z)));
#
print(`(b) cos coefficients`);
ZERO:=expand((op(1,op(3,[test[0]]))+op(1,op(3,[test[1]]))+op(1,op(3,[test[2]]))+
op(1,op(3,[test[3]]))+op(1,op(3,[test[4]])))/(I*alpha*cos((1-sub)*gamma*z)));
#
#
print(`N=2, v-equation:`);
print(`------------------`);
print(`(a) sin coefficients`);
ZERO:=expand((op(2,op(2,[test[0]]))+op(2,op(2,[test[1]]))+op(2,op(2,[test[2]]))+
```

```
op(2,op(2,[test[3]]))+op(2,op(2,[test[4]])))/(I*alpha*sin((2-sub)*gamma*z)));
#
print(`(b) cos coefficients`);
ZERO:=expand(factor(op(2,op(3,[test[0]]))+op(2,op(3,[test[1]]))+
op(2,op(3,[test[2]]))+op(2,op(3,[test[3]]))+op(2,op(3,[test[4]])))/
(I*alpha*cos((2-sub)*gamma*z)));
#
print(`and so on...`);
print();
# now for the omega equation:
if(mode=3)then
  test[0]:=find_trig(expand(equom_0),6,mode):
  test[1]:=find_trig(expand(equom_1),6,mode):
  test[2]:=find_trig(expand(equom_2),6,mode):
  test[3]:=find_trig(expand(equom_3),6,mode):
  test[4]:=find_trig(expand(equom_4),6,mode):
else
  test[0]:=find_trig(equom_0,6,mode):
  test[1]:=find_trig(equom_1,6,mode):
  test[2]:=find_trig(equom_2,6,mode):
  test[3]:=find_trig(equom_3,6,mode):
  test[4]:=find_trig(equom_4,6,mode):
fi:
#
print(`----------------------II----------------------------------------`);
print(`N=0, eta-equation:`);
print(`------------------`);
ZERO:=expand((op(1,op(1,[test[0]]))+op(1,op(1,[test[1]]))+op(1,op(1,[test[2]]))+
op(1,op(1,[test[3]]))+op(1,op(1,[test[4]])))/(I*alpha));
#perhaps some collect or so ...
#
print(`N=1, eta-equation:`);
print(`------------------`);
print(`(a) sin coefficients`);
ZERO:=expand((op(1,op(2,[test[0]]))+op(1,op(2,[test[1]]))+op(1,op(2,[test[2]]))+
op(1,op(2,[test[3]]))+op(1,op(2,[test[4]])))/(I*alpha*sin((1-sub)*gamma*z)));
#
print(`(b) cos coefficients`);
ZERO:=expand((op(1,op(3,[test[0]]))+op(1,op(3,[test[1]]))+op(1,op(3,[test[2]]))+
op(1,op(3,[test[3]]))+op(1,op(3,[test[4]])))/(I*alpha*cos((1-sub)*gamma*z)));
#
#
print(`N=2, eta-equation:`);
print(`------------------`);
print(`(a) sin coefficients`);
ZERO:=expand((op(2,op(2,[test[0]]))+op(2,op(2,[test[1]]))+op(2,op(2,[test[2]]))+
op(2,op(2,[test[3]]))+op(2,op(2,[test[4]])))/(I*alpha*sin((2-sub)*gamma*z)));
#
print(`(b) cos coefficients`);
ZERO:=expand(factor(op(2,op(3,[test[0]]))+op(2,op(3,[test[1]]))+
op(2,op(3,[test[2]]))+op(2,op(3,[test[3]]))+op(2,op(3,[test[4]])))/
(I*alpha*cos((2-sub)*gamma*z)));
#
print(`and so on...`);
```

```
print();
#-----------------solve for the other components of velocity -------------
print(‘other velocity components are:‘);
print(‘-----------------------------‘);
#ss:=solve({equcont=0,defeta=etat(y,z)},{un(y),wn(y)});
ss:=solve({subs({sum_from_one=1},equcont)=0,subs({sum_from_one=1},defeta)=
subs({sum_from_one=1},etat(y,z))},{un(y),wn(y)});
arg1:=op(2,op(1,ss)):
arg2:=op(2,op(2,ss)):
```